CASCADE PERFORMANCE OF A DOUBLE ARC COMPRESSOR BLADE AT LOW REYNOLDS NUMBER

by

Urs Jakob Keller

Thesis submitted to the Graduate Faculty of the Virginia Polytechnic Institute and State University in partial fulfillment of the requirements of the degree of

MASTER OF SCIENCE

in

Mechanical Engineering

APPROVED:

H. L. Moses, Chairman

W. F. O'Brien, Jr.

H. L. Wood

October 1978

Blacksburg, Virginia

II. ACKNOWLEDGMENTS

The author expresses sincere appreciation to members of his advisory committee: Professors H. L. Wood, W. F. O'Brien, Jr., and H. L. Moses, Chairman. Dr. Moses was especially helpful throughout the investigation.

The support which was received from funds of the M.E. Department at VPI&SU and a scholarship of the Swiss Federal Institute of Technology in Zurich, sponsored by BBC Brown, Boveri & Company, Ltd., Baden, Switzerland, is also acknowledged.

The author expresses his appreciation to and for their helpful assistance during the final investigation. He is also grateful for the wind-tunnel equipment, manufactured by the M. E. workshop. The author is also indebted to Sandy Hubbard for her patient and professional typing of the thesis.

Finally, the author is very indebted to his wife for her constant encouragement and support.

III. TABLE OF CONTENTS

Table of Contents Cont.

IV. LIST OF FIGURES

List of Figures Cont.

V. LIST OF TABLES

VI. LIST OF SYMBOLS

a_n	coefficients used in Eq. (5)
a_{ij}	coefficients used in Eqs. (7) and (8)
b_{ij}	coefficients used in Eqs. (7) and (8)
c	speed of sound
h	stream tube characteristic
H_{12}	shape factor = δ_1/δ_2
i	incidence angle
k	ratio of specific heats
ℓ	blade height
L	chord
M	Mach number
p	pressure
Re	Reynolds number
s	pitch
u	velocity component in x-direction
U	freestream velocity at edge of boundary layer
v	velocity component in y-direction
V	freestream velocity
V_1	air inlet velocity
V_2	air outlet velocity
w	total pressure loss = $p_{01} - p_{02}$
$\bar{w}$	mean total pressure loss
x	chordwise direction

List of Symbols Cont.

y	direction perpendicular to blade chord line
α_1	air inlet angle
α_1'	blade inlet angle
α_2	air outlet angle
α_2'	blade outlet angle
β	velocity profile shape factor
γ	stagger angle
δ	boundary layer thickness
δ_1	displacement thickness
δ_2	momentum thickness
δ_α	deviation angle
ε	deflection angle = $\alpha_1 - \alpha_2$
$\bar{\varepsilon}$	mean deflection angle
θ	blade chamber angle
ρ	density
ψ	stream function

subscripts

$\circ$	signifies stagnation state
i	mesh point index in x-direction
j	mesh point index in y-direction

VII. INTRODUCTION

Since engineers have been involved in constructing turbomachines such as axial-flow compressors, special attention has been paid to the design of the blading. This part of the compressor is responsible for the conversion of the proper work at the shaft into the fluid [1]*. In order to improve this process, a considerable amount of research has been done during the past years. The major objective was, and still is, the complete understanding of the fluid flow through cascades, single stages and multistages.

Experimental and analytical methods have been used to overcome the difficulties in predicting two-dimensional and three-dimensional flow in turbomachines. One of the most important parts of such predictions is how accurately one can determine the resulting overall loss [2]. At the present time, the competition in the turbomachinery market becomes more and more intense. Even fractions of percentage points of efficiency, beside financing and other aspects, can determine whether a product will be competitive or not. Therefore it is of importance to know the nature, origin and magnitude of all possible losses [3]. Only in this manner will it be possible to improve the effectiveness of a stage and finally of an entire machine.

Continuing investigations in areas such as stall and surge, compressibility, boundary layer effects, three-dimensional effects, etc., are being conducted, to explain and calculate losses. But no

---

*Numbers in brackets designate References at the end of the thesis.

unique theory has ever been developed that would handle such a complex problem. Rather than a single explanation, several small theories, combined in a complete work, will lead to a better understanding of the mechanism of loss.

One way to predict a fraction of the entire loss, namely the so-called profile loss, is by means of two-dimensional studies which involve cascade tests on the one hand and flow field calculations on the other. Here, and in other countries, much experimental research has been devoted to cascade tests on compressor blading. In addition, analytical flow calculations have been improved to a degree that one can develop new cascades without extended cascade tests. But there is still information on phenomena, such as boundary layer transition and separation, that only can be gained by experiment.

The purpose of this study is to test a compressor cascade at a low Reynolds number. This investigation results in two main items of information: (i) the angle through which the air is turned, and (ii) the corresponding profile drag or profile loss coefficient from which the cascade efficiency may be estimated [4]. A recently-developed computer program to calculate the free stream and boundary layer simultaneously [5] is applied to a compressor cascade. The results are compared with experimental data.

VIII. LITERATURE REVIEW

The complexity and three-dimensional character of the flow through axial compressors and fans led to the reduction of the problem into two dimensions. Even though effects such as tip clearance leakage, hub and casing shear, etc., cannot be included in two-dimensional cascade studies, a qualitative judgment on a blade row can be achieved by determination of the profile loss. That is, a cascade of high two-dimensional performance will also perform well when applied in a turbomachine. This fact, beside others, justifies the emphasized two-dimensional flow research.

A. Two-Dimensional Cascade Tests

The limited possibilities in the field of flow calculations about two-dimensional blade sections and the advantages of stationary models gave rise to extended cascade tests in the 1940's. In the United States, NACA engineers collected data on a large scale during that time [6]. The British, namely Carter and Howell, also started fundamental cascade investigations in 1946 [7].

The variety of wind-tunnels used to conduct the experiments made a correlation of the results impossible. One of the most difficult problems was to establish a true two-dimensional flow in the test section. The application of large settling chambers, screens and honeycombs to equalize the flow, and contracting sections to reduce the boundary layer thickness improved the results from wind-tunnels [8]. The removal of the boundary layer upstream and within

the blade row, already discovered by Prandtl in 1904 [9], found its application in cascade testing in 1950 [10], [11]. In order to guarantee a periodic flow in a blade row, several successful techniques have been developed. Slots in the end walls, a very simple and effective solution, have been used by Carter, Andrews and Shaw in their studies beginning in 1950 [11], whereas flexible sidewalls in high speed cascades have been applied by the Deutsche Forschungsanstalt fuer Luftfahrt in Braunschweig since 1956 [8]. Just recently, Stephens [23] of Pratt & Whitney Aircraft, used tailboards to influence the flow in the wind-tunnel. All of these improvements resulted in more consistent test data. The comparison between theoretical and experimental performance in the two-dimensional field became more significant as mentioned by Lieblein [12].

In recent times, great efforts have been made by Pollard and Gostelow [13], Roberts [14], Ross and Bohne [15] in investigating the influence of variation of parameters such as Reynolds number, free-stream turbulence, aspect ratio, axial velocity ratio, sound-level, etc., on test results. The conclusion of these and other studies are summarized as follows:

Sidewall boundary layer removal at low aspect ratio will give good two-dimensional results.

The criterion of axial velocity ratio equal to unity is reliable.

Using solid sidewalls, an aspect ratio of at least three is recommended in order to obtain two-dimensional flow.

High free-stream turbulence level delays the increase in loss at low Reynolds numbers.

The cascade deviation angle varies linearly with axial velocity ratio.

Generally, seven or more blades are recommended when testing cascades.

As the Reynolds number decreases, there is a critical point where profile loss and deviation angle increase.

Sound-wave type disturbances ("noise") are the most important type of unsteadyness in some transonic wind-tunnels. Additional noise causes transition to occur more forward, but there is no evidence that the boundary layer development depends on the accoustical disturbances at low noise levels.

The basic objective of cascade tests is to evaluate the blade row performance. For the purpose of illustrating collected data, different correlation procedures have been developed by Howell, Carter, and the NACA [15]. In this report, the method of Howell, which relates deflection angle and total pressure loss directly to the incidence angle is used. In order to compare measured and calculated blade velocity distributions, all of the velocities are expressed in fractionsof inlet-velocity and plotted against the fractionsof chord, a manner widely used in turbomachinery literature.

B. Two-Dimensional Flow Calculation

In addition to time-consuming and expensive experimental studies, engineers have also attempted to calculate the two-dimensional cascade flow. Various types of flow-idealizations, such as steady state, non viscous, incompressible, irrotational, etc., led to the development of different methods to find the flow characteristics for a given cascade. According to Roudebush [17], this so-called "direct problem" was first solved by means of conformal mapping. But only blade cascades of simple shape could be solved and less accuracy was achieved for arbitrary profiles. The application of singularities such as sinks, sources and vortices made possible a calculation of the flow through a blade cascade of any geometrical form. Especially the method of superimposing point vortices on the profile contour and a uniform flow is still successfully applied. Significant improvements in this method have been carried out by Imbach in 1964 [18] and Van den Braembusch in 1977 [19]. The introduction of modern computers opened the field for relaxation and matrix solutions. Katsanis and McNally, as well as others, developed a blade-to-blade Fortran program for calculating velocities and stream lines on a stream surface, using a finite difference method [20]. A similar procedure to calculate the flow-field was applied by Jones [21] in a computer solution for the two-dimensional flow through a compressor blade cascade, handling the compressible case and including the viscous flow.

In order to predict a cascade characteristic, it is necessary to consider the boundary layer flow along the profile contour. Since the AFOSR-IFP-Stanford 1968 Conference on "Computation of Turbulent Boundary Layers", a milestone in the history of boundary layer theory, no pioneering new method to describe this complex shear flow has been found. Only minor improvements have been contributed in order to complete already existing theories. Basically the same findings of Prandtl, Schlichting etc., are applied to solve turbomachinery boundary layer problems. The method used in the current investigation was developed by Moses in 1964 and is an integral type of boundary layer solution [22].

The superposition of the inviscid flow solution and the result of the boundary layer calculation is the most common method applied. An iteration procedure is required that recalculates both solutions considering new profile contours, set by the boundary layer displacement thickness. The convergence of the procedure is not guaranteed in all cases. However, in 1978, Moses et al. [5] calculated the freestream and the boundary layer simultaneously for a diffusing passage. The same type of solution which involves great advantages concerning the singularity at the separation point and instabilities within the separated region, is applied in the computer program used, and partially described, in this report.

IX. EXPERIMENTAL EQUIPMENT

The experiments have been conducted in an open-circuit wind-tunnel. A schematic layout of the experimental apparatus is shown in Fig. 1; and a pictorial view is presented in Fig. 2. The apparatus consists of three major parts: (i) the wind-tunnel, (ii) the cascade test section and (iii) the measuring equipment. Whereas the tunnel and the measuring instruments already existed, the entire test-section had to be designed and built.

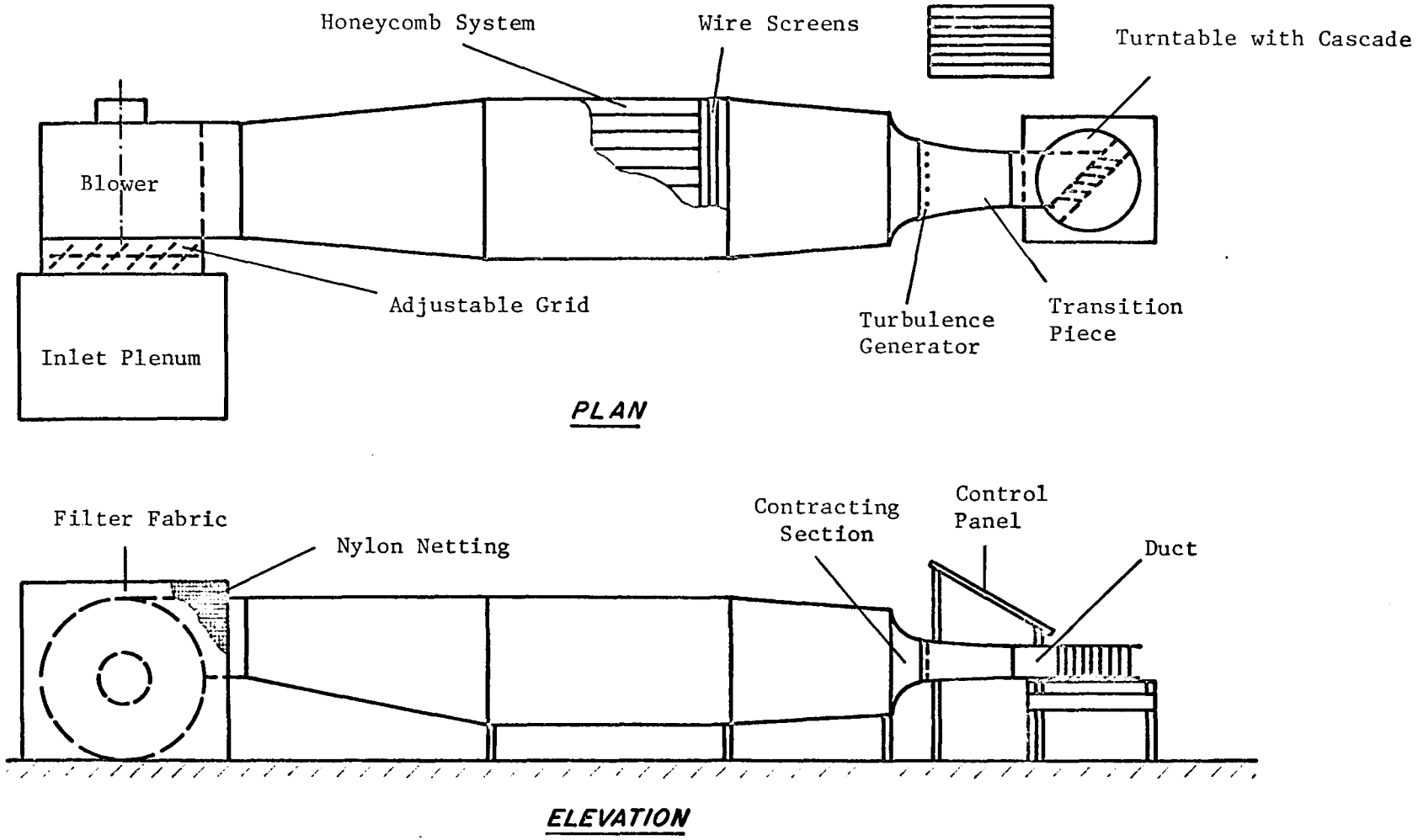

Fig. 1 Schematic layout of the experimental apparatus

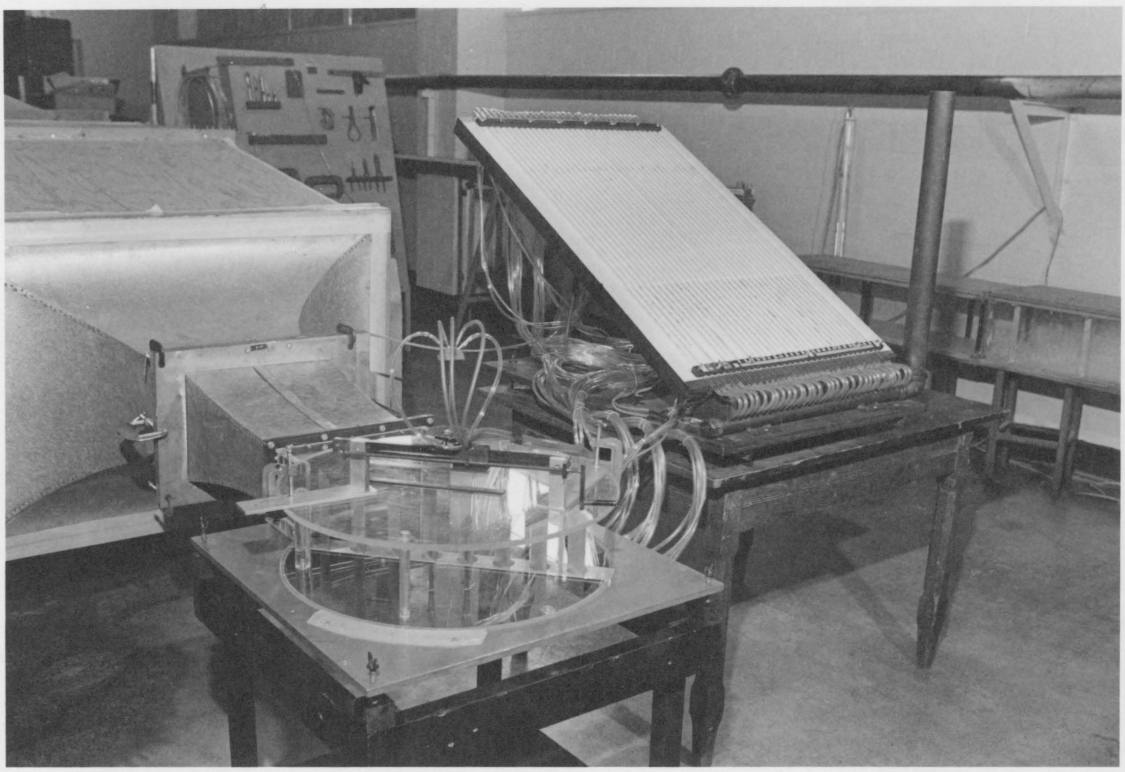

Fig. 2 Experimental Apparatus

A. The Wind-Tunnel

An inlet plenum, covered with nylon nettings and filter fabric, produces an inlet flow to the blower with no distortion originating in the surroundings and guarantees a constant mass flow. Between the plenum and the blower, an adjustable grid controls the inlet velocity to the cascade test section. The compressor, a centrifugal blower with an installed power of 13.4 kw (10.0 Hp), delivers the air to the connected tunnel. Uniform flow is produced by a honeycomb system consisting of 1.3m long paper tubes with an inner diameter of 50 mm and a wall thickness of 2 mm. A series of three wire screens with a mesh size of 2 mm and a wire diameter of 0.2 mm reduces the freestream turbulence to 0.5 percent. The final contracting section accelerates the flow and prevents the growth of boundary layers on the channel walls.

B. The Cascade Test Section

The test section is connected to the wind-tunnel by means of a slightly contracting transition piece. Five vertically aligned paper tubes at the inlet of the transition piece generate a free-stream turbulence of 4.3 percent, estimated to be of the same order as the turbulence level occuring in a compressor. The tubes with an outer diameter of 30 mm cover 45 percent of the inlet cross section area. The inlet duct, designed as short as possible to prevent excessive boundary layer growth, is 65 mm long and 127 mm x 304 mm in cross section. This duct is directly coupled to a turntable

system on which the blade cascade is installed. The turntable, consisting of two rotary discs, can be set at different positions. This permits a change in the inlet flow angle relative to the blades, even while operating the wind-tunnel. Details of the blade cascade are given in the next section.

With the present apparatus the maximum velocity in the cascade is about 42 m/s, which corresponds to a Mach number of 0.12 and a Reynolds number, based on the blade chord length, of 1.8×10^5.

C. The Blade Cascade

The cascade consists of eight double circular arc-type compressor blades which are made of Epoxy resin. A description of the blade mold and blade fabrication technique is given in the Appendices. The cross section, as shown in Fig. 3, closely approximates a scaled mid-span cross section of a first stage rotating compressor blade in a General Electric T64-GE-6B gas turbine. All the blades are straight and have a span of 127.0 mm and a chord of 65.53 mm. The principal geometric parameters of the cascade are as follows:

(i) aspect ratio $\frac{\ell}{L} = 1.94$

(ii) pitch-chord ratio $\frac{s}{L} = 1.00$

(iii) stagger angle $\gamma = 36.5°$.

Two of the blades are provided with 12 static pressure taps each. These taps are placed on the suction side of one blade and the pressure

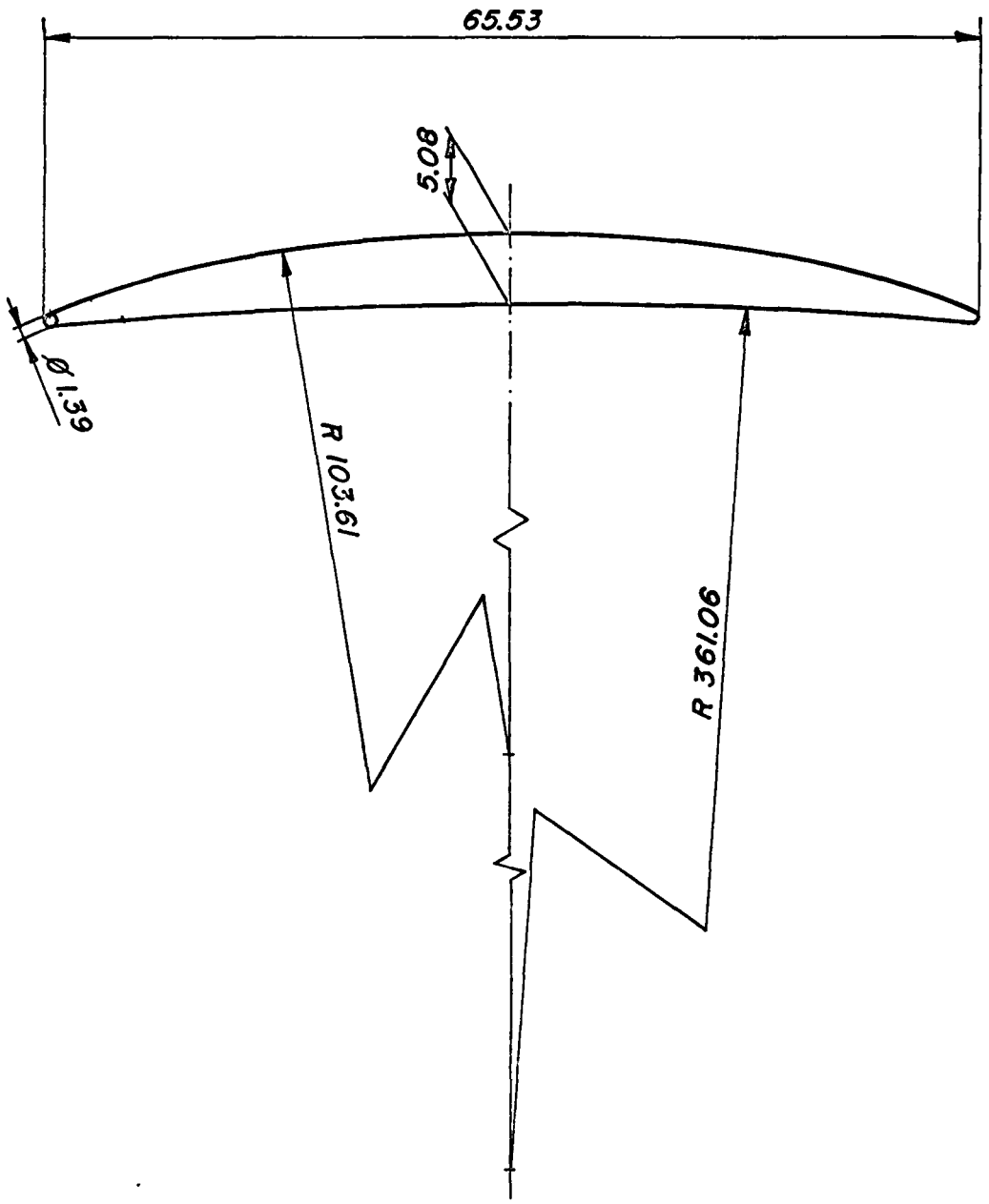

Fig. 3 Blade profile

side of another blade. Location and numbering of the taps are shown in Fig. 4 and Fig. 5. The blades are placed in adjacent positions at the center of the cascade. In this region, the desired periodicity and the two-dimensional character of the flow field is expected to be more likely than in the outer region of the blade cascade. A pictorial view of the blade row is shown in Fig. 6. All the angles and dimensions used to characterize the cascade and to describe geometric flow conditions are given in Fig. 7.

D. The Measuring Equipment

The main measuring instrument used in this investigation is a 5-hole cobra head yaw probe type DC-125, manufactured by the United Sensors & Control Corp. Massachusetts. This probe was employed to measure the mid-span periodicity of the flow one chord length upstream of the cascade as well as the total pressure and flow direction 2.0 mm downstream of the blades. The probe is mounted on a traverse which allows angular readings of 1/5 of a degree and traversing readings of 1/4 of a millimetre. The mechanism to traverse the probe is shown in Fig. 8. Before starting the experiments, the 5-hole probe was calibrated.

The leads of the probe, as well as those of the pressure taps, are connected to a multitube inclined manometer, as shown in Fig. 2. This manometer has a bank of 32 tubes and is filled with water. The manometer assembly is inclined by 60°. This arrangement allows pressure readings down to 0.25 mm of water to be ascertained.

A hotwire anemometer system, manufactured by Thermo-Systems Inc., and the yaw probe were simultaneously applied to determine the freestream turbulence level. A schematic view of the probe arrangement is shown in Fig. 9.

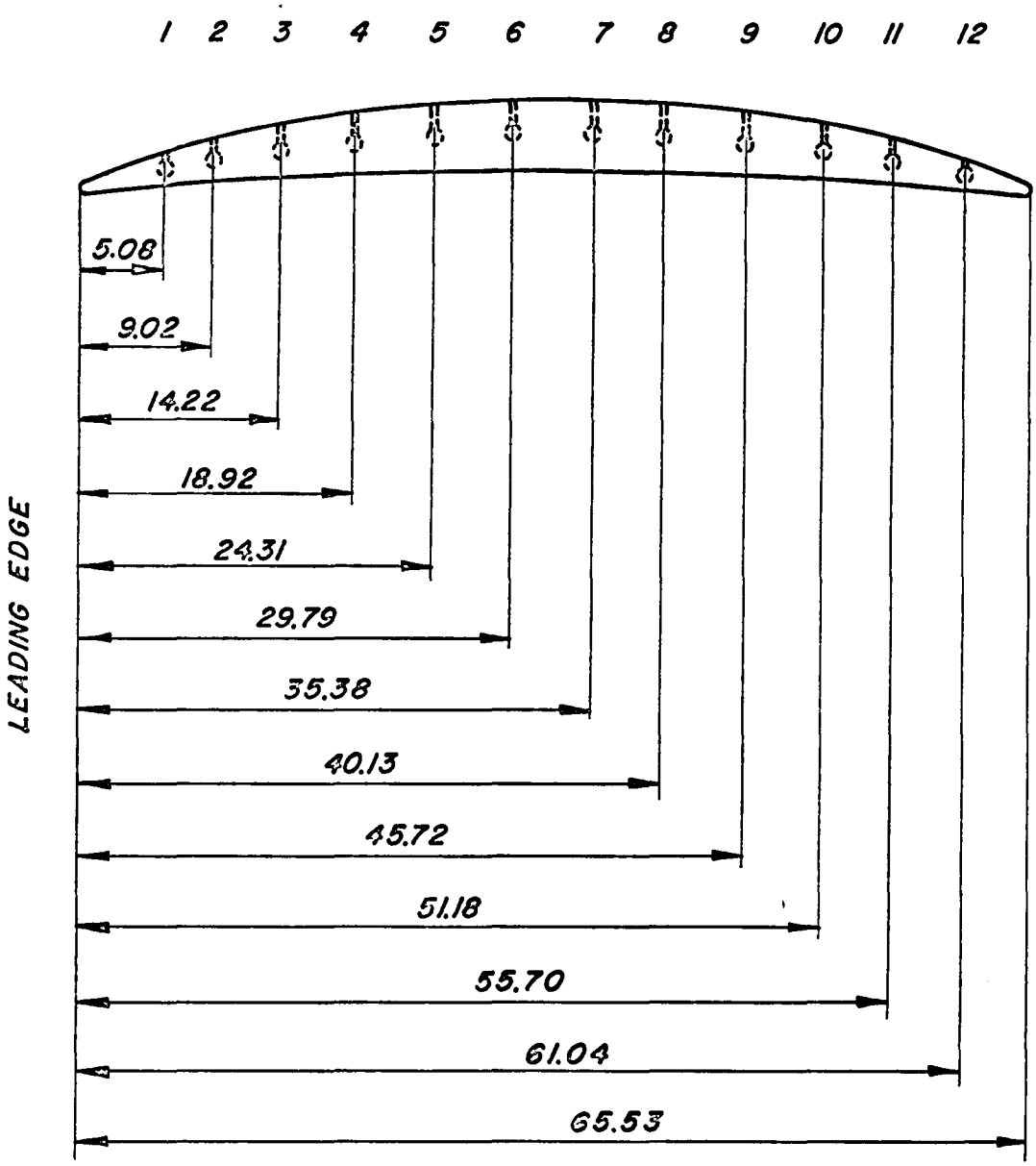

Fig. 4 Static pressure taps on suction side

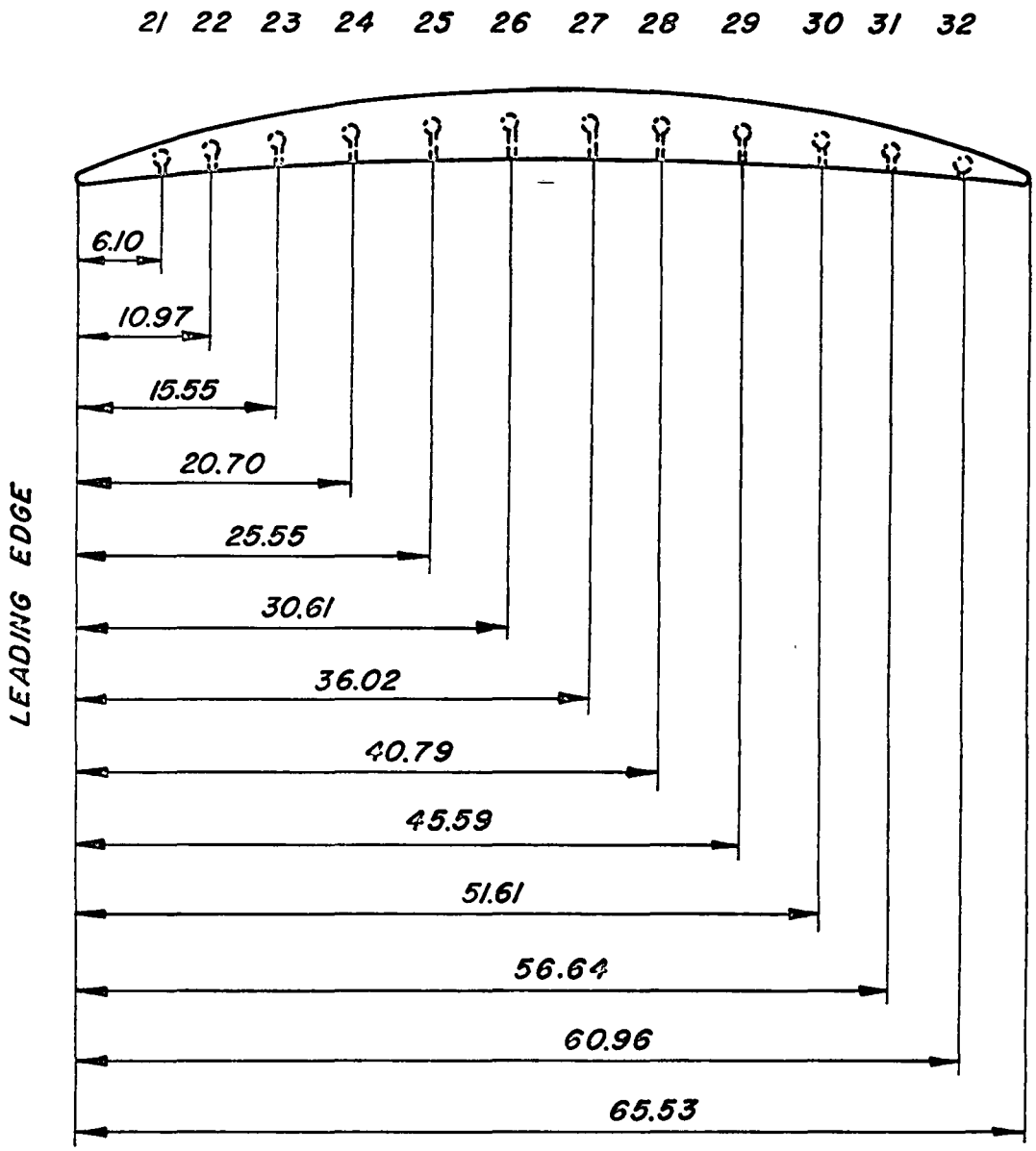

Fig. 5 Static pressure taps on pressure side

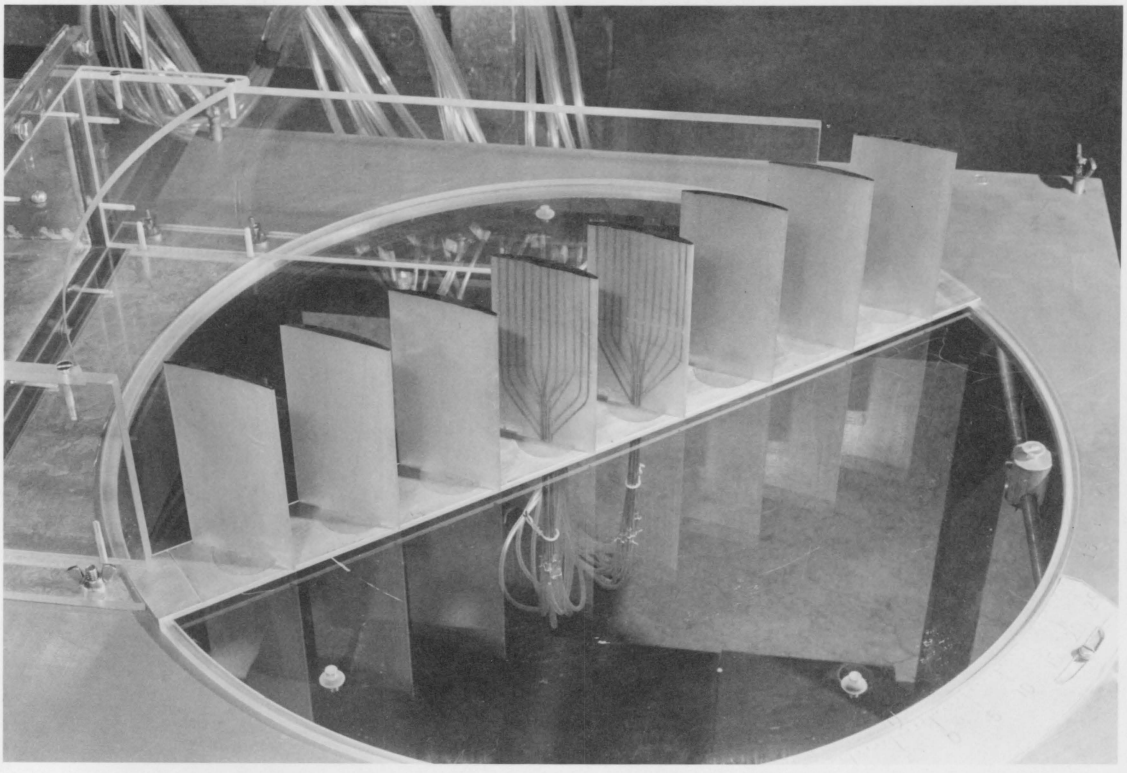

Fig. 6 Blade Cascade

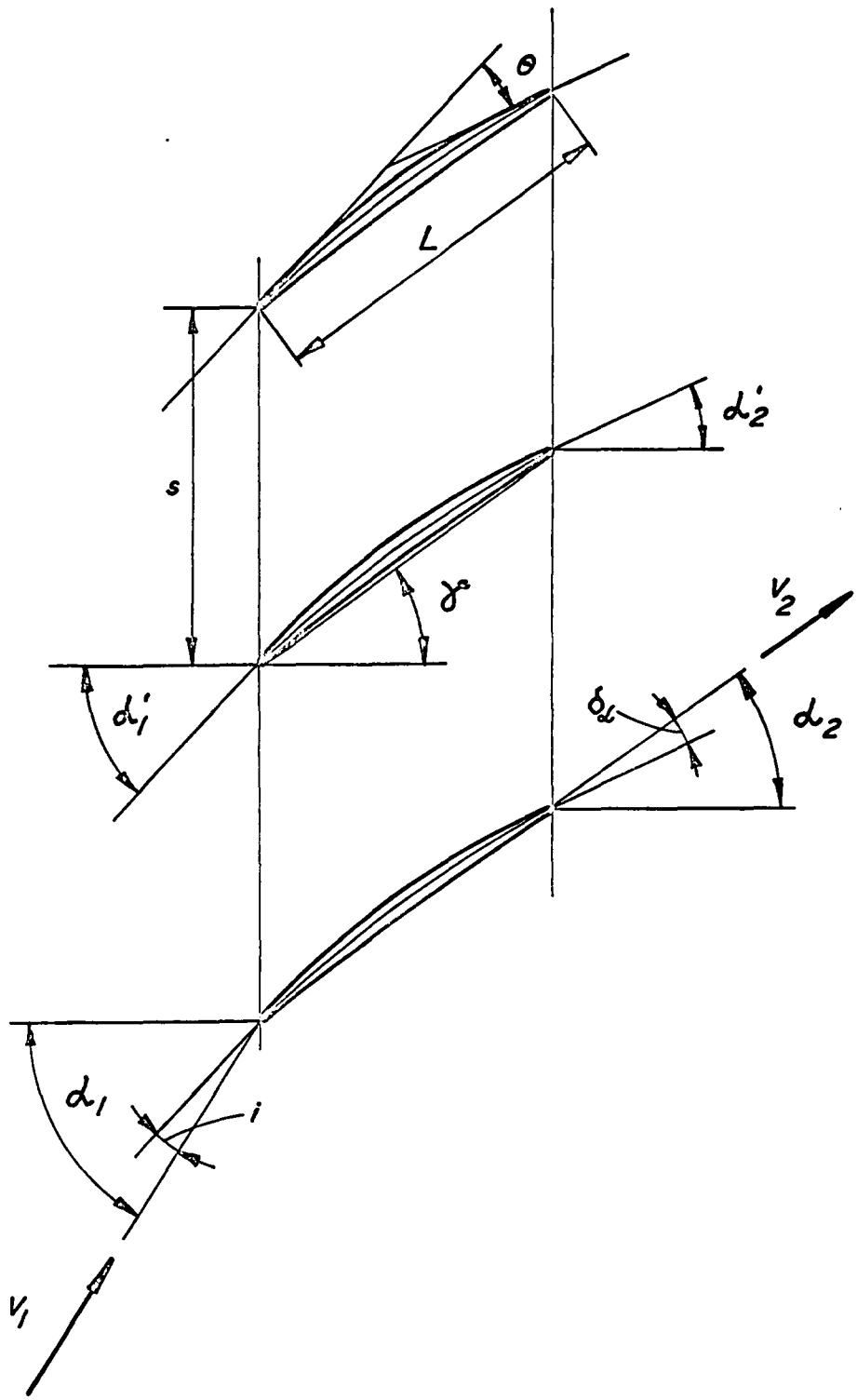

Fig. 7 Cascade notation

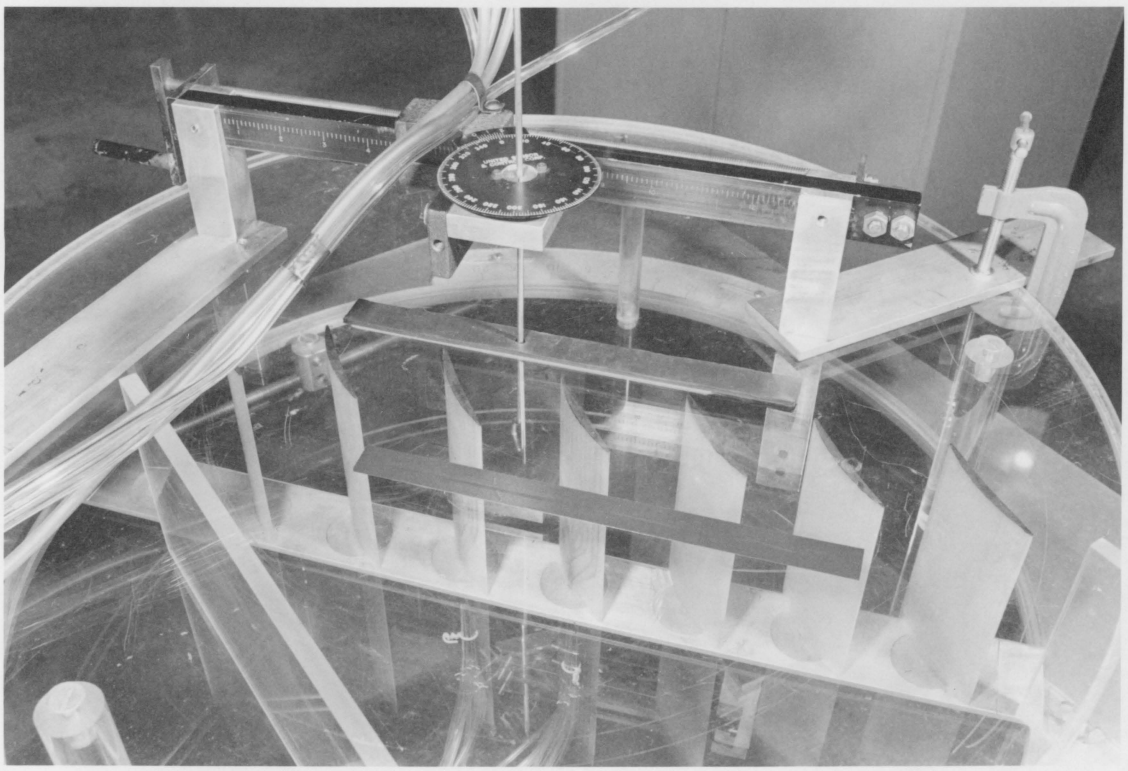

Fig. 8 Probe Traverse

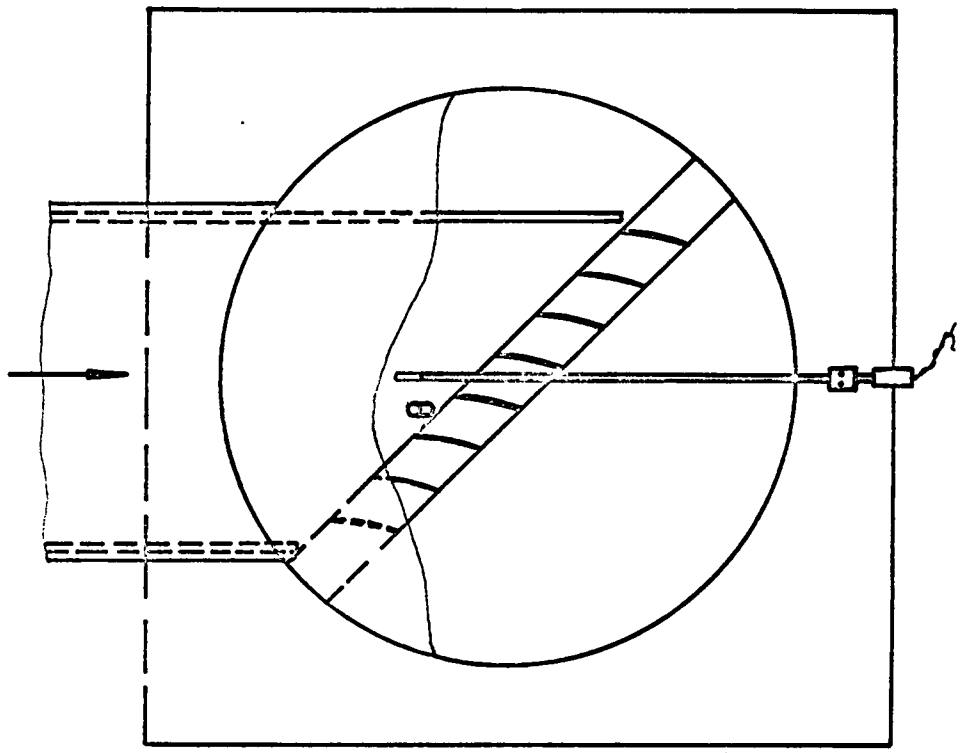

PLAN

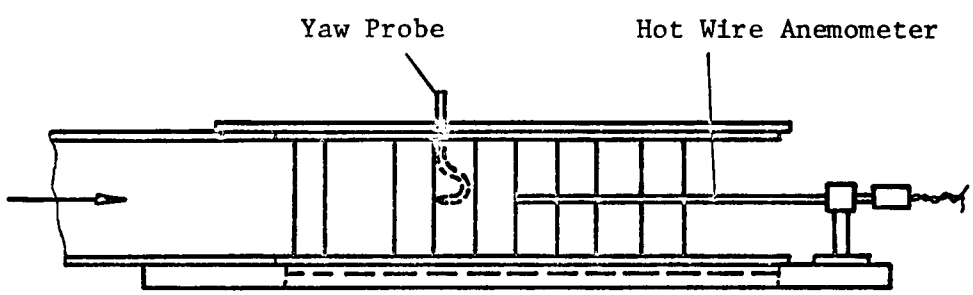

ELEVATION

Fig.9 Hot wire and yaw probe arrangement

X. COMPUTER ANALYSIS

It is not the purpose of this report to give a detailed description of the computer program, which is thoroughly discussed in reference 21. However, a brief outline that indicates the main theories and methods applied should impart the necessary understanding.

In order to solve the flow through a specified compressor cascade (direct problem), three major flow regions have to be considered.

(i) the inviscid flow region,

(ii) the boundary layers near the blade surface, and

(iii) the endwall boundary layers.

In this case, the first two flow regions are treated independently but solved simultaneously. The endwall boundary layers are accounted for through a stream tube contraction factor.

A. The Inviscid Flow

The inviscid flow under investigation is assumed to be:

(i) steady relative to the blades,

(ii) quasi-three dimensional,

(iii) irrotational, and

(iv) compressible.

In addition,

(v) the velocity magnitude and direction are uniform over the upstream and downstream boundaries,

(vi) the velocities normal to the blades are zero, and

(vii) there is no heat transfer within the area of investigation.

Taking all these assumptions into account, the resulting differential equation for the stream function for subsonic flow in cartesian coordinates reads:

$$\left[1 - \left(\frac{\rho_o}{\rho}\right)^2 \left(\frac{h_o}{h}\right)^2 \frac{\psi_y^2}{c^2}\right] \psi_{xx} + \left[1 - \left(\frac{\rho_o}{\rho}\right)^2 \left(\frac{h_o}{h}\right)^2 \frac{\psi_x^2}{c^2}\right] \psi_{yy}$$

$$+ 2 \left(\frac{\rho_o}{\rho}\right)^2 \left(\frac{h_o}{h}\right)^2 \frac{\psi_x \psi_y}{c^2} \psi_{xy} = o \qquad (1)$$

where, for isentropic flow,

$$c^2 = c_o^2 - \frac{k-1}{2} \left(\frac{\rho_o}{\rho}\right)^2 \left(\frac{h_o}{h}\right)^2 (\psi_x^2 + \psi_y^2) \qquad (2)$$

$$\frac{\rho_o}{\rho} = \left[1 + \frac{k-1}{2} M^2\right] \frac{1}{k-1} \qquad (3)$$

$$M^2 = \frac{V^2}{c^2} = \frac{u^2+v^2}{c^2} = \left(\frac{\rho_o}{\rho}\right)^2 \left(\frac{h_o}{h}\right)^2 \frac{\psi_x^2+\psi_y^2}{c^2} \qquad (4)$$

The differential equation (1) is solved by means of a finite difference method. Fig. 10 shows the grid system applied in the computer program. In general, the mesh is not square.

The solution procedure used for the finite difference calculation is a successive line relaxation (SLR) method. In this approach, the unknowns at each value of i (see Fig. 11) are determined simultaneously, with values at i-1 from the preceding calculation and i+1 from the previous iteration. For any value of i, the equations

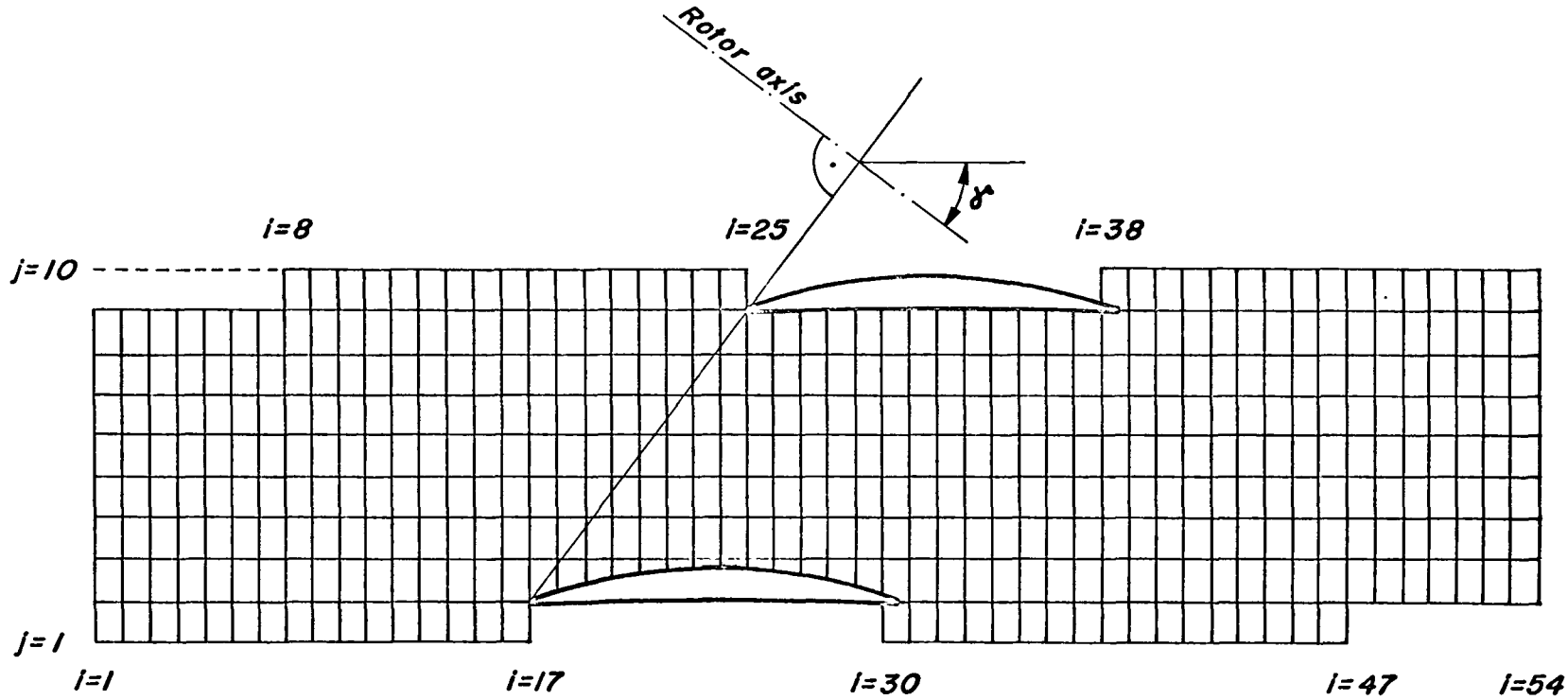

Fig. 10 Grid system for inviscid flow region

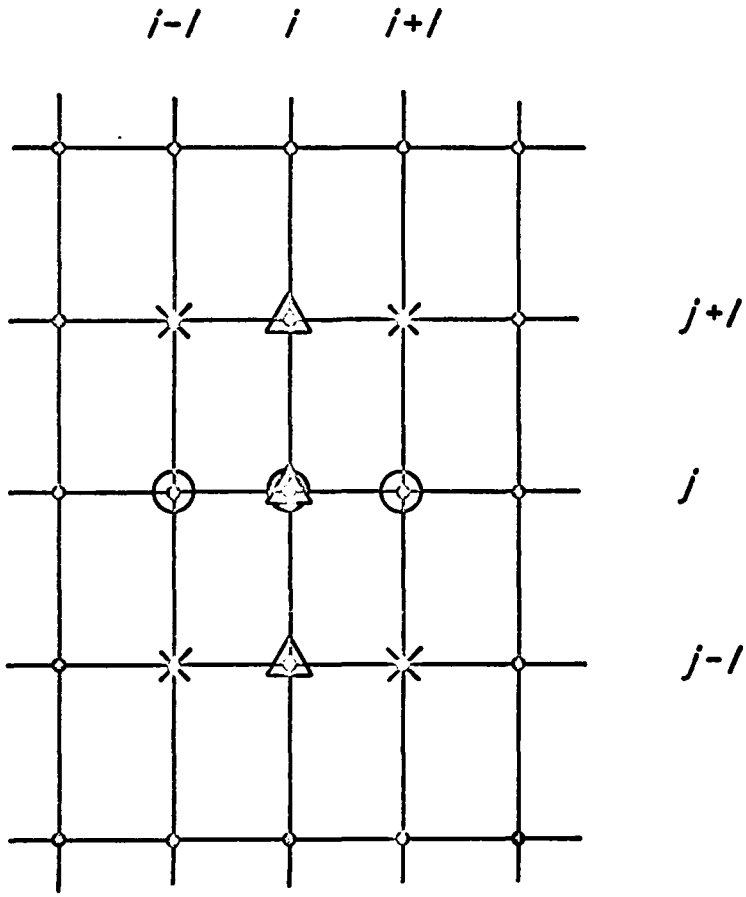

ψ_{xx}, ψ_x involves ○

ψ_{yy}, ψ_y involves △

ψ_{xy} involves ×

Fig. 11 Section of grid system

can be written

$$a_1\psi_{i,j-1} + a_2\psi_{i,j} + a_3\psi_{i,j+1}$$

$$= a_4 - a_5[\psi_{i+1,j+1} - \psi_{i-1,j+1} - \psi_{i+1,j-1} + \psi_{i-1,j-1}]$$

$$- a_6[\psi_{i+1,j+1} - \psi_{i-1,j}] \qquad (5)$$

The coefficients a_n are functions of the grid spacing and initial thermo- and fluid dynamic data. Since the resulting matrix is tri-diagonal, the set can be solved by means of a simple algorithm. To avoid numerical difficulties for nodal points near the blade surface, a grid line shifting procedure is applied.

Since in the mathematical sense the present problem is of elliptical character, the boundary conditions must be prescribed completely around the area of interest. This means that a first approximation for the air outlet angle α_2 has to be specified; and an iteration procedure is introduced to satisfy the "trailing edge condition".

B. The Boundary Layers

To solve the boundary layer equations, a two-parameter integral method is applied. The velocity profile assumption is in parametric form and reads as follows

$$u/U = f(y/\delta, \beta) \qquad (6)$$

where δ is the boundary layer thickness and β is a profile shape parameter. For the laminar boundary layer, either a cubic, quartic or Falkner-Skan velocity profile can be applied. The turbulent boundary layer is calculated by means of either power law profiles, logarithmic profiles or a series of modified logarithmic velocity profiles. An empirical relation is employed for the dissipation integral. The modified logarithmic series of profiles also includes separated flow. To account for the wake, an overall displacement thickness is determined at the trailing edge and used in calculating the potential flow downstream.

For the unknown parameters, ordinary differential equations are derived by integrating the boundary layer equation in y across the boundary layer. The resulting equations for laminar and turbulent flow are of the form,

$$a_{11}d\delta + a_{12}d\beta = b_{11}dU + b_{12}ds \tag{7}$$

and

$$a_{21}d\delta + a_{22}d\beta = b_{21}dU + b_{22}ds \tag{8}$$

The parabolic character of the boundary layer equations and a known freestream velocity distribution allow a numerical solution by means of a stepwise procedure in the downstream direction. At the point of separation, most boundary layer calculations fail since the determinant of the coefficient matrix a_{ij} is zero (the equations become singular) and a solution only exists for a specific pressure gradient. Thus, the pressure cannot be previously specified with

sufficient accuracy to avoid infinite derivatives at this point.

To overcome the numerical difficulties at separation, the boundary layer equations are solved simultaneously with the free-stream.

C. The Simultaneous Solution of the Boundary Layer and Freestream

Because of the elliptic character of the freestream, which requires an iteration procedure, the simultaneous solution is not straightforward. The procedure followed in the computer program is that of SLR as applied to the solution of the freestream. By arranging all equations, including those for the boundary layer, so that the coefficient matrix is tridiagonal, the reduction of the computational time is considerable. A detailed description of the equation system and the boundary conditions is given in references 5 and 21. Written in matrix format, the coupled equations describing the boundary layer for pressure and suction side and the freestream take the form shown in Fig. 12.

Based on the resulting boundary layer data at the trailing edge, the theoretical profile loss is calculated by means of the equation given by Lieblein [12]:

$$\frac{\overline{w}}{\frac{1}{2}\rho V_1^2} = 2\left(\frac{\delta_2}{L}\right)\frac{L/s}{\cos\alpha_2}\left(\frac{\cos\alpha_1}{\cos\alpha_2}\right)^2\left(\frac{2H_{12}}{3H_{12}-1}\right)\left[1 - \left(\frac{\delta_2}{L}\right)\frac{(L/s)H_{12}}{\cos\alpha_2}\right]^{-3} \qquad (9)$$

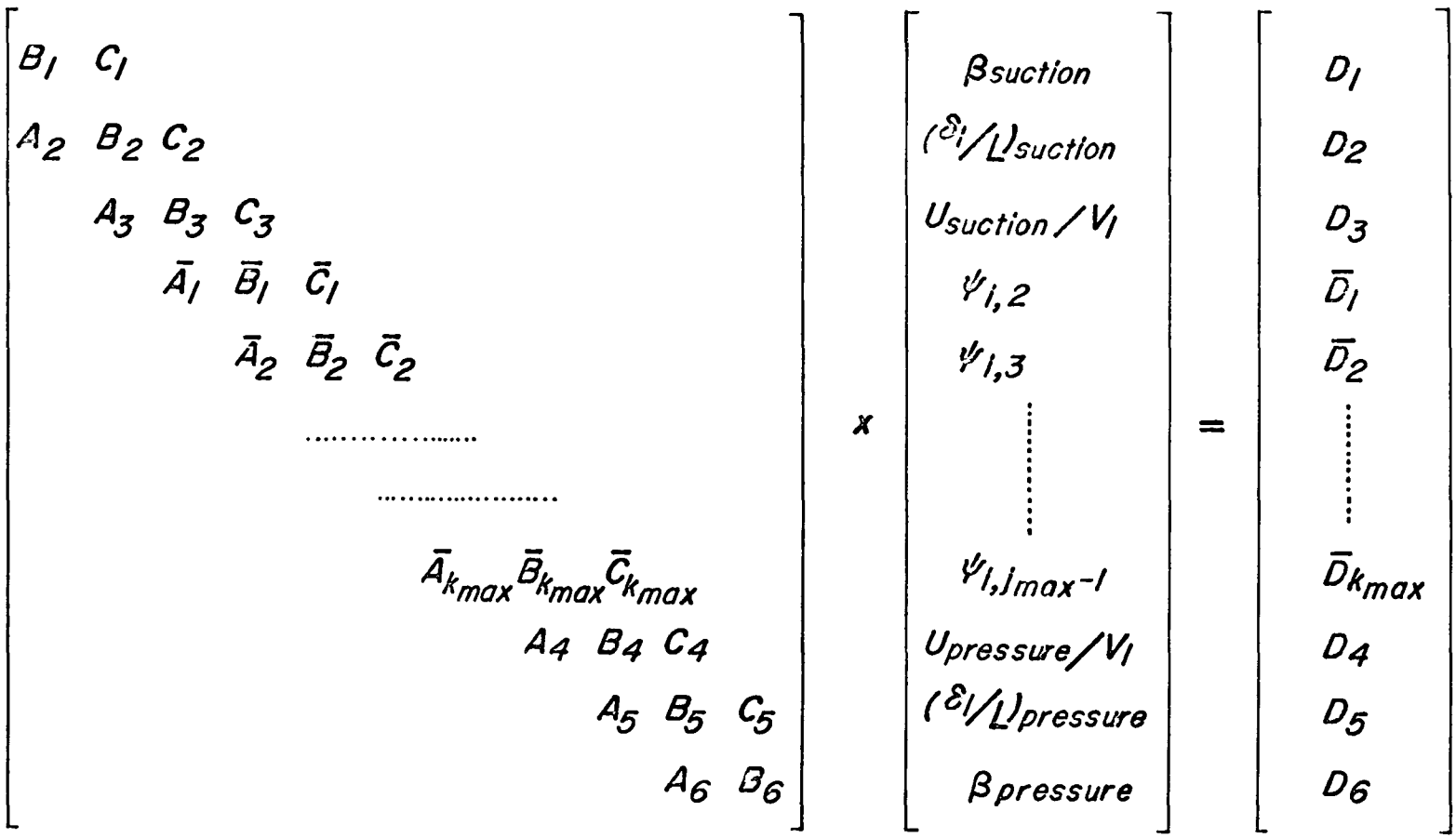

A, $\bar{A}$, B, $\bar{B}$, C, $\bar{C}$, D, and $\bar{D}$ are coefficients based on the grid system and flow parameters.

Fig. 12 Coupled equations in matrix format

XI. RESULTS

The blade cross section under investigation was tested at different incidence angles ranging from -12.6 degrees to +12.0 degrees. Because of the blockage effect of the cascade at large negative incidence angles and the limited fan power, the Reynolds and Mach number varied slightly over the range of incidence angles, as shown in Table 1.

In order to compare analytical and experimental data for the velocity distribution along the blade surface, the results for three different incidence angles ($i = +9.0°$, $i = +0.6°$ and $i = -12.6°$) are shown in Figures 13 through 15. The computer calculations do not account for the stream tube contraction and assume turbulent flow beginning at the leading edge. The initial values chosen to start the boundary layer calculation are 1.55 for the shape factor H_{12} and 6.55×10^{-2} millimetres for the displacement thickness δ_1 at 7.44 percent of chord. The experimental data were taken at a freestream turbulence level of 4.3 percent.

Figure 16 shows the influence of introducing a streamtube contraction factor based on the axial velocity ratio on the analytical results for the velocity distribution at $i = +0.6°$. The axial velocity ratio was derived from measurement of the flow field one chord upstream and just downstream of the trailing edge of the blade. The streamtube contraction through the blade passage is simulated in the computer program by a cubic polynomial and approximates measured flow

contractions shown in reference 13.

An example of the results derived from the wake measurements is shown in Fig. 17. A description of the calculation procedure for the final experimental profile loss is shown in the Appendices. A summary of all the profile losses and deflection angles resulting from the experiments at different angles of incidence is shown in Fig. 18. The same figure also shows the theoretical results calculated by means of the current version of the computer program.

Since all the experiments were carried out at low Reynolds numbers, the free stream turbulence level had to be increased from 0.61 percent to 4.5 percent in order to avoid laminar flow and separation. The effect of this step on the velocity distributions, profile losses and deflection angles is shown in figure 19 and 20.

Table 1 Mach number and Reynolds number for different incidence angles

Incidence angle (degrees)	Mach number ( )	Reynolds number ( )
12.0	0.114	1.526×10^5
9.0	0.115	1.518×10^5
7.0	0.114	1.526×10^5
3.0	0.114	1.531×10^5
0.6	0.115	1.525×10^5
- 3.0	0.112	1.525×10^5
- 6.0	0.113	1.519×10^5
- 9.0	0.108	1.430×10^5
-12.6	0.105	1.397×10^5

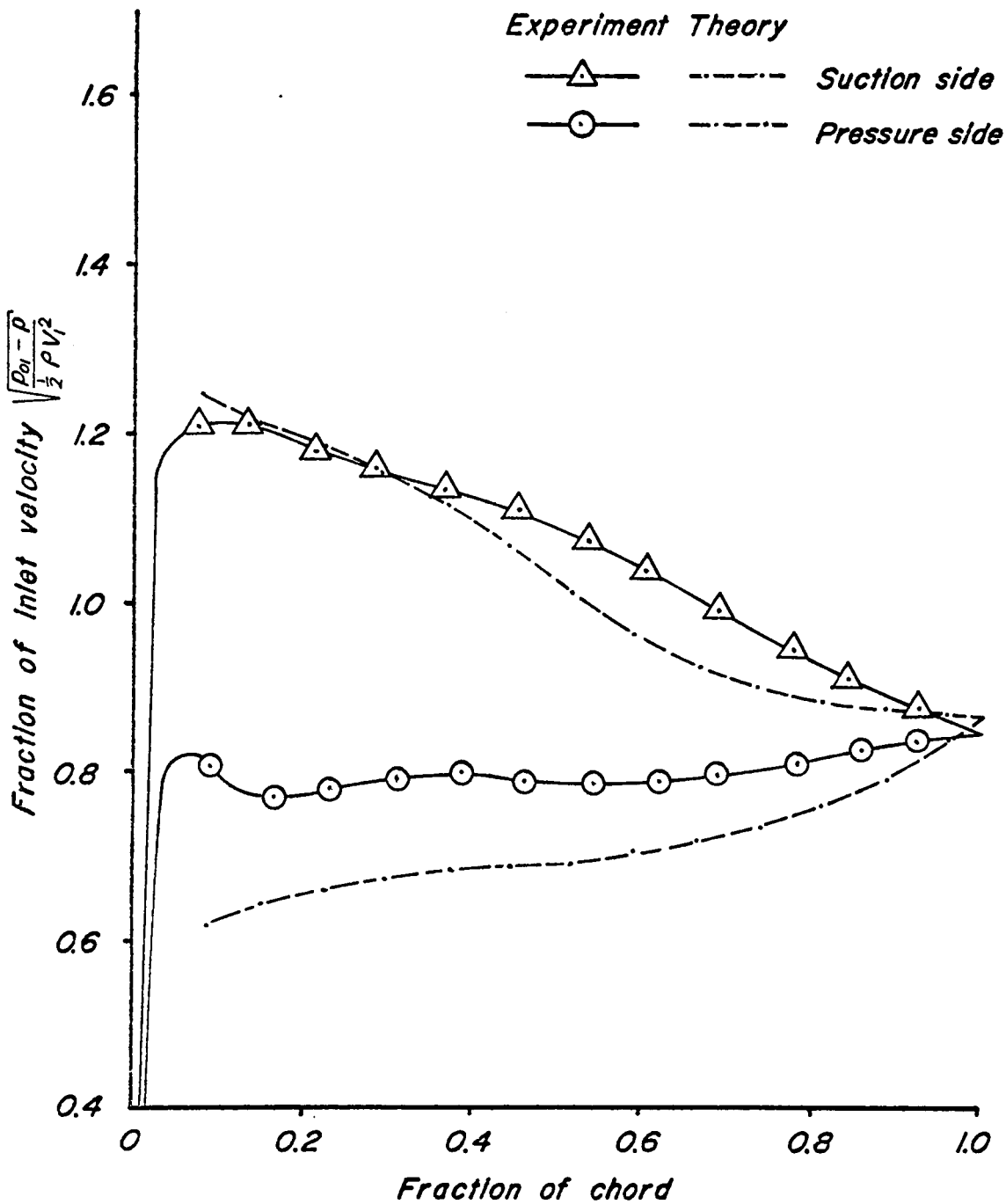

Fig. 13 Velocity distribution for i = +9.0°,

Re = 1.518 x 10^5 and M = 0.115

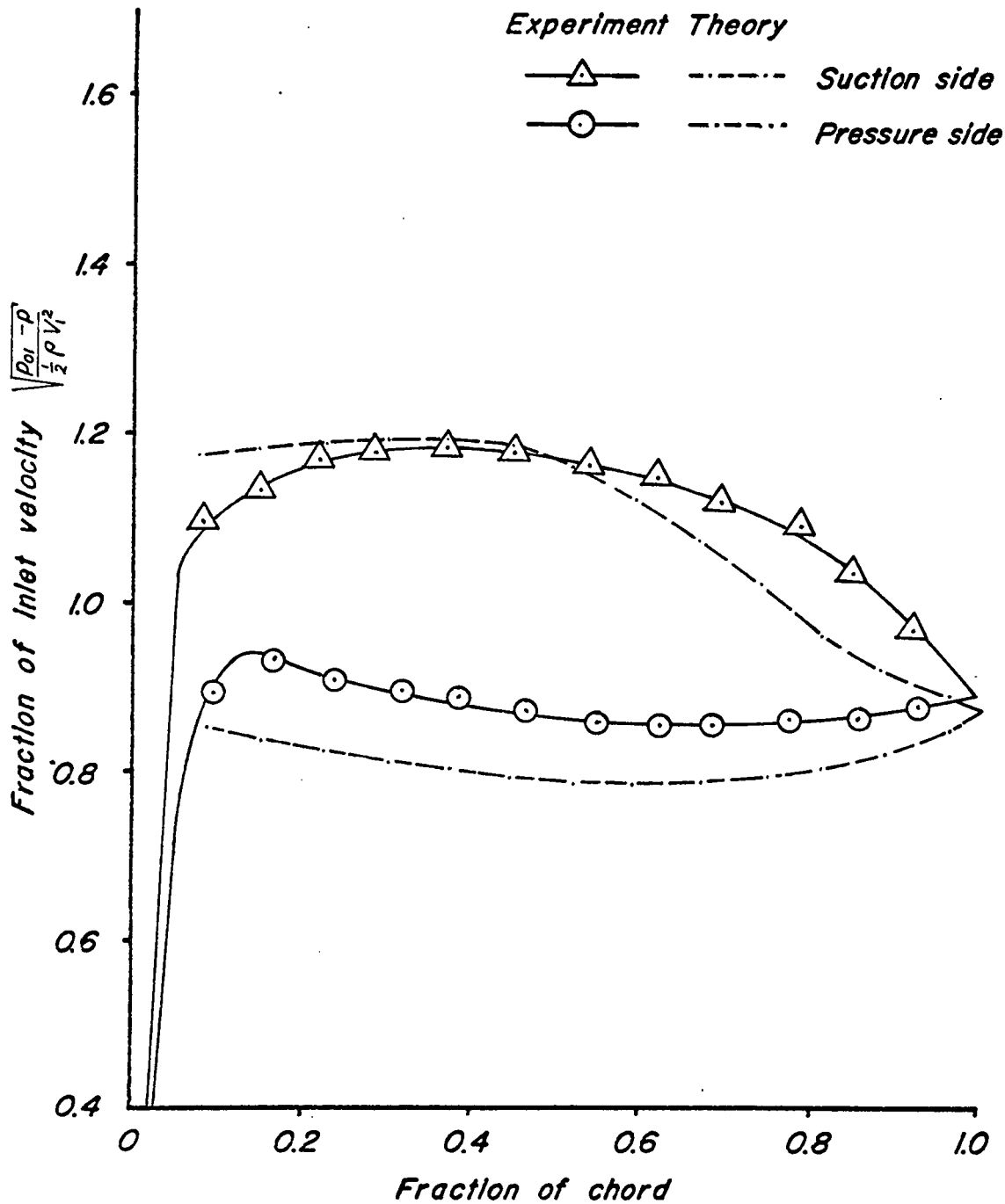

Fig. 14 Velocity distribution for i = +0.6°

Re = 1.525 x 10^5 and M = 0.115

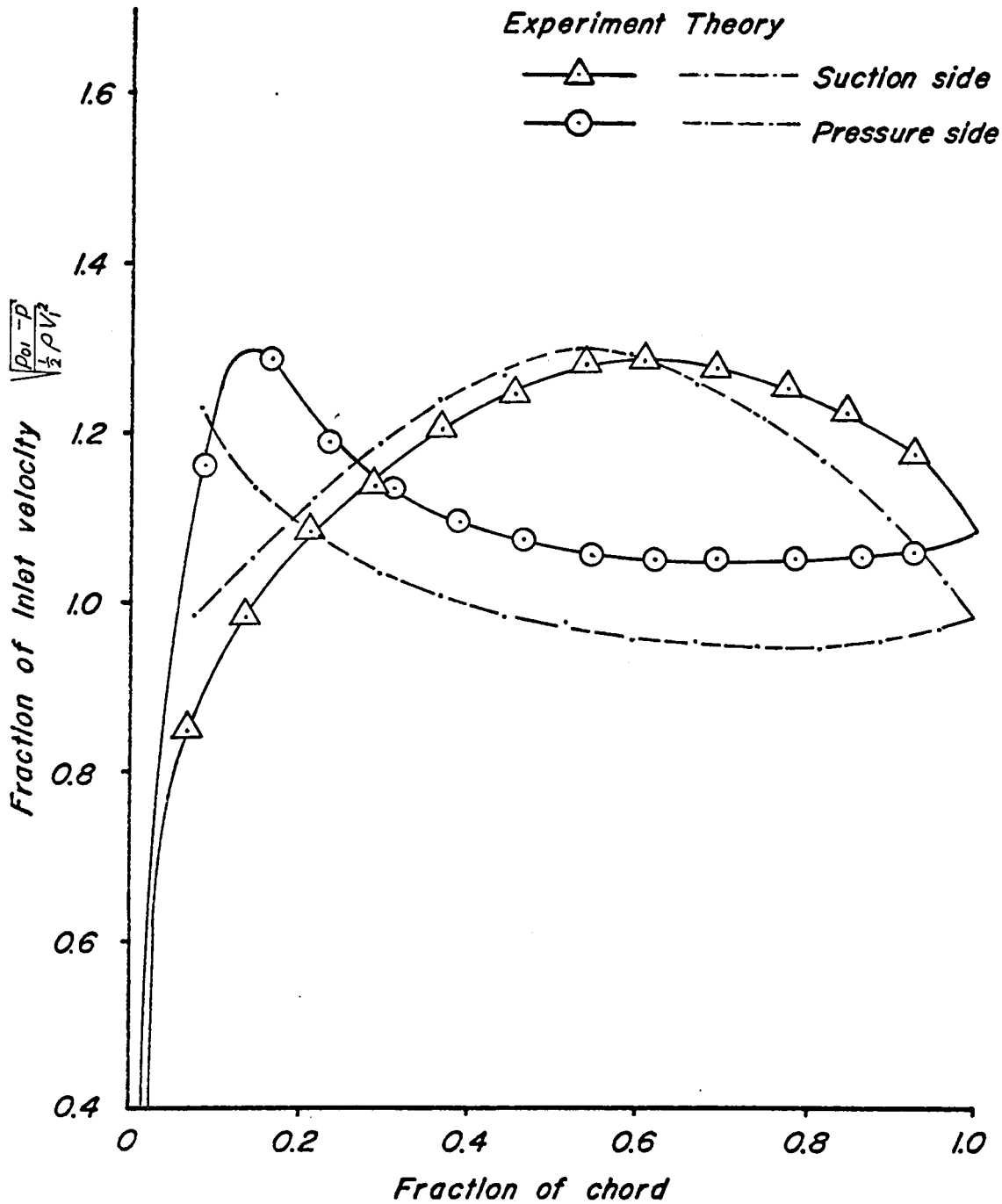

Fig. 15 Velocity distribution for i = -12.6°,

Re = 1.397 x 10^5 and M = 0.105

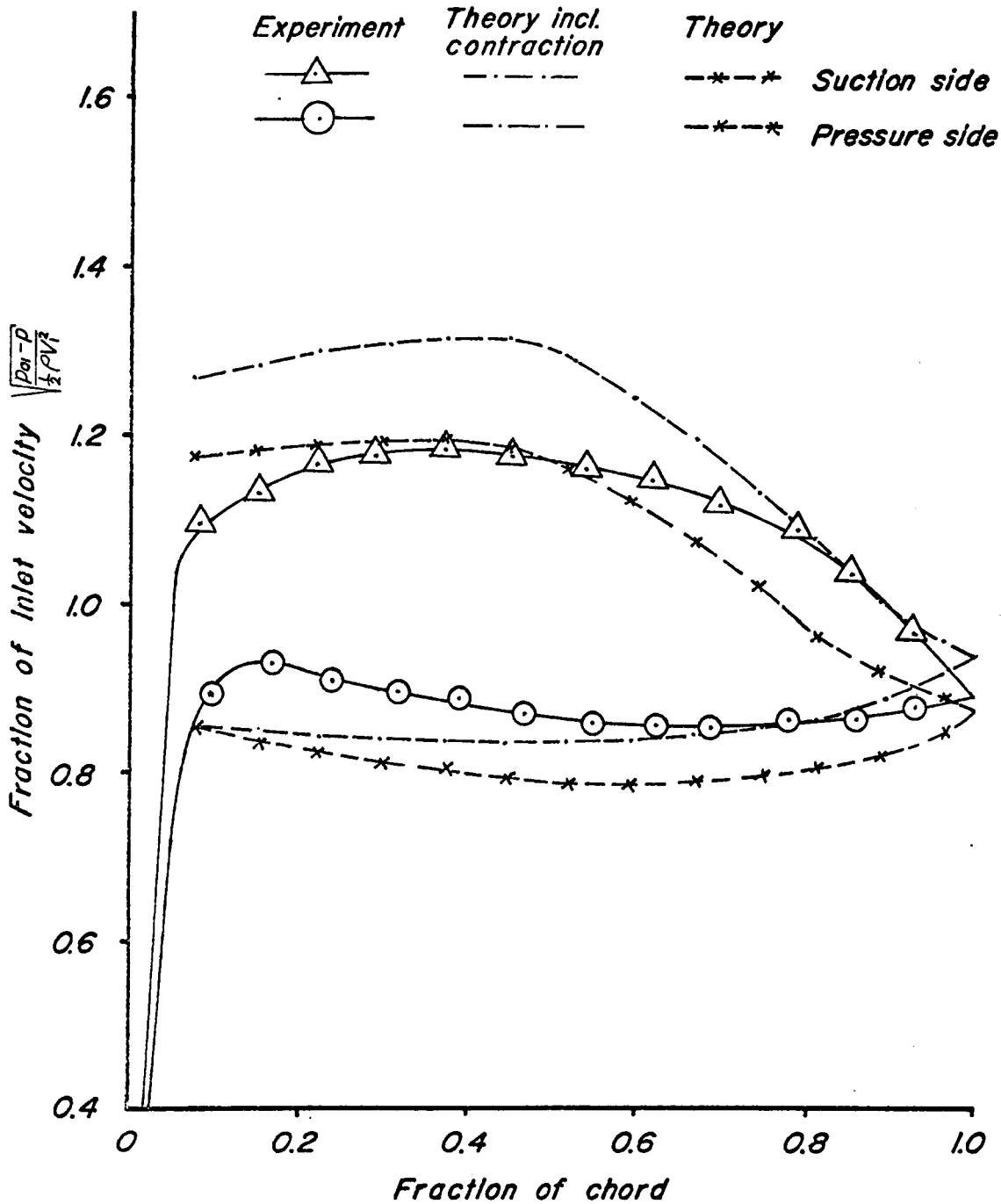

Fig. 16 Influence of the stream tube contraction factor on the theoretical velocity distribution for $i = +0.6°$, $Re = 1.525 \times 10^5$ and $M = 0.115$

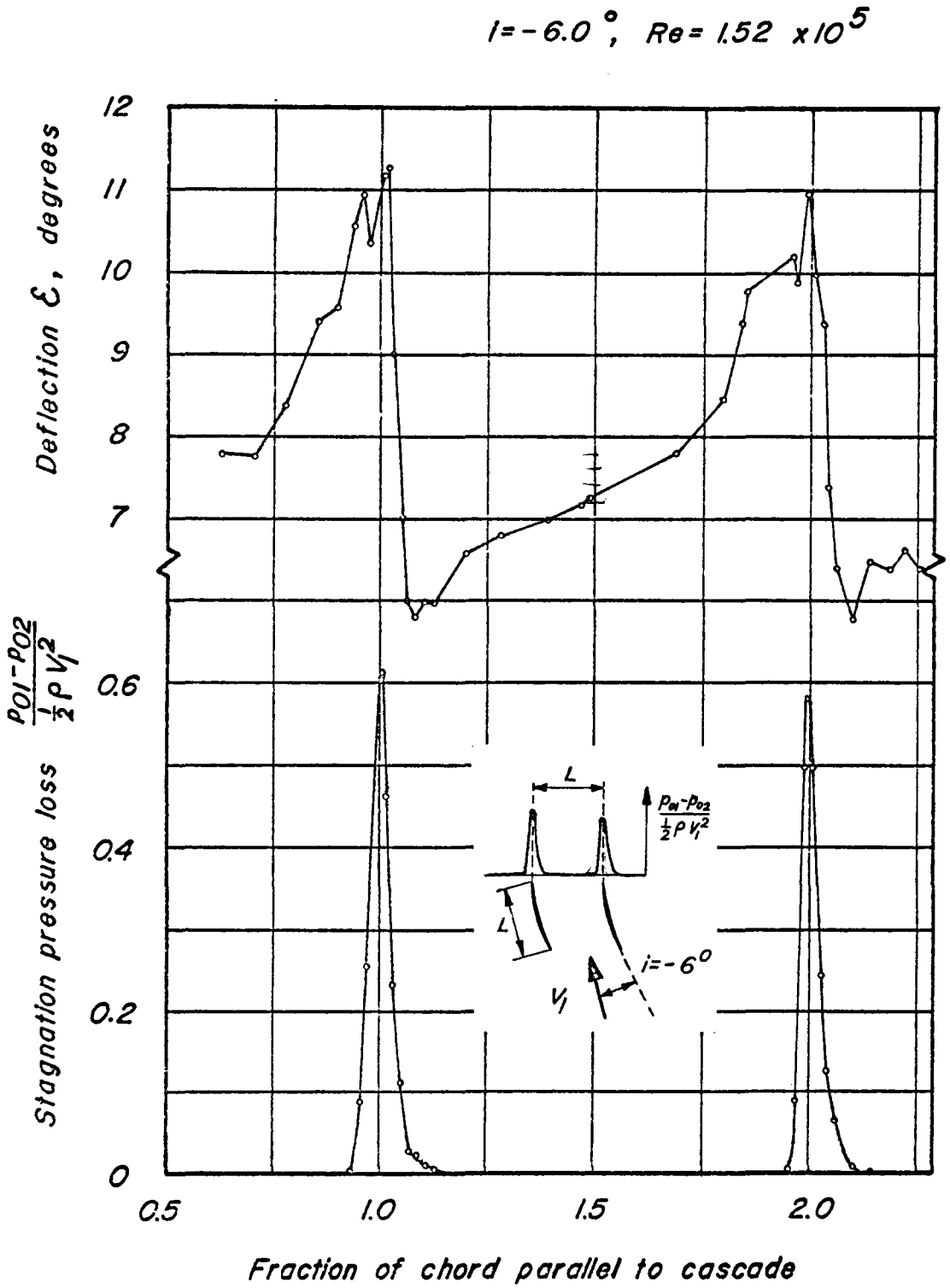

Fig. 17 Stagnation pressure loss and deflection

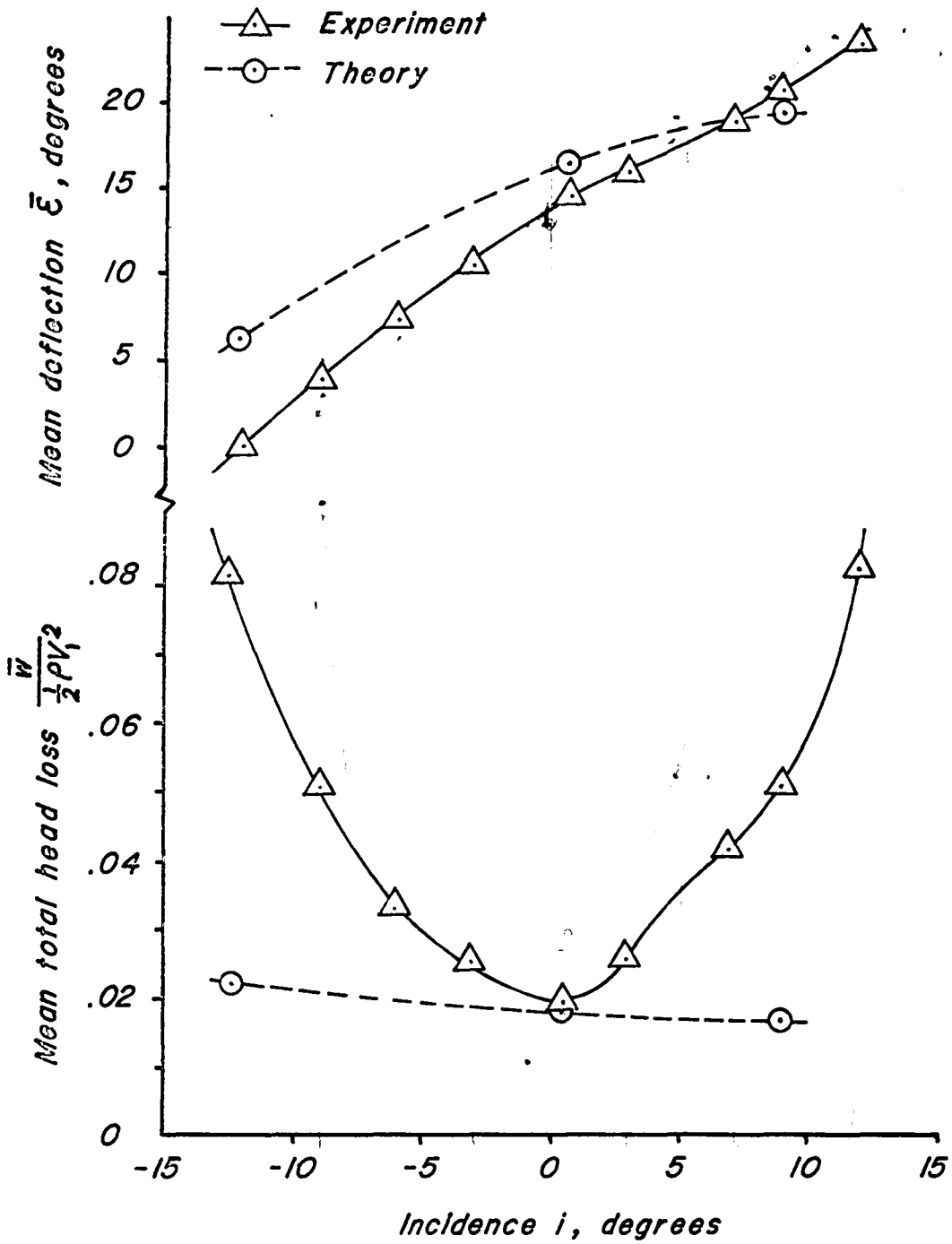

Fig. 18 Mean deflection and mean total head pressure loss for different angles of incidence

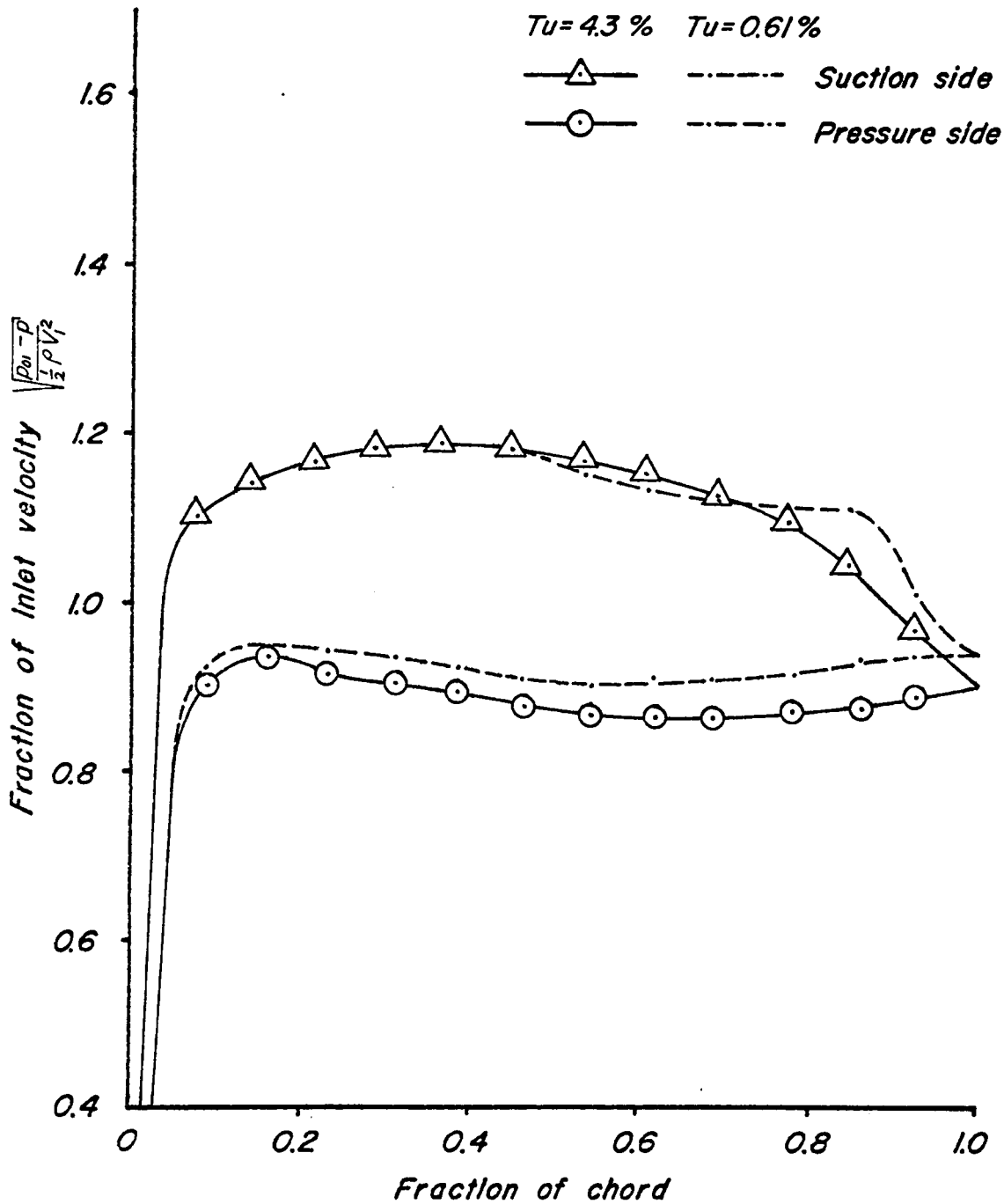

Fig. 19 Experimental velocity distribution along blade surface at different turbulence levels for i = 0.6°, Re = 1.525 x 10^5 and M = 0.115

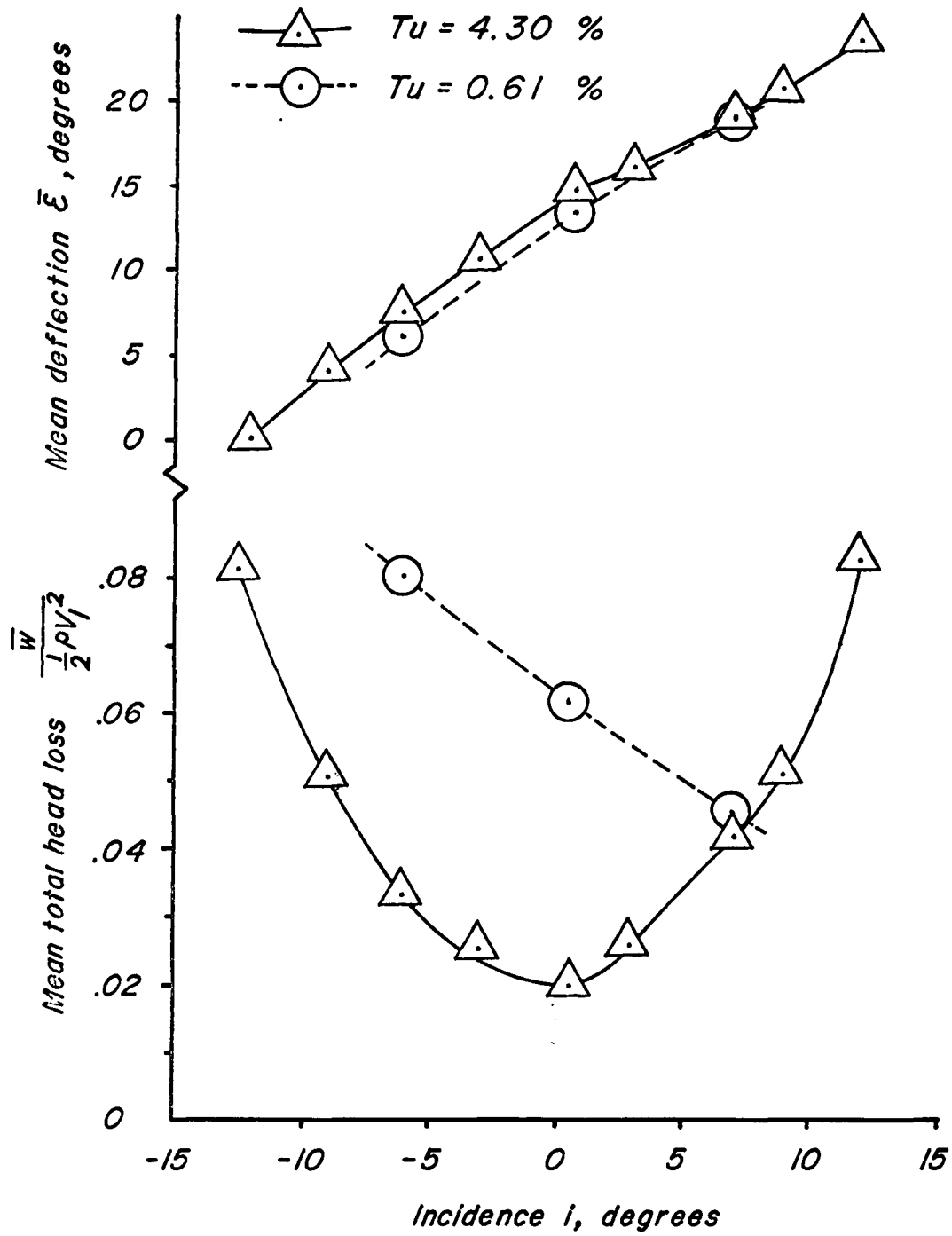

Fig. 20 Mean deflection and mean total head pressure loss for different levels of turbulence

XII. DISCUSSION

A comparison of experimental and theoretical results for the velocity distribution along the blade surface at various incidence angles is presented in Figures 13 through 15. The calculated distributions in general follow the trend established by the experimental curves. The calculated suction side curve matches the experimental curve beginning from the leading edge up to 50 percent of chord, where it decreases more rapidly than the measured values. This is partially due to the stream tube contraction within the experimental blade passage, caused by the endwall boundary layers, which increases the experimental velocity readings. Another reason for the difference is the application of the power law for the velocity profiles in the turbulent boundary layer calculations. The power law type of boundary layer velocity profiles do not account for even small amounts of backflow and are limited to unseparated flows. Even though it appears that no separated regions are visible on the plots in Figures 13 through 15, small amounts of backflow, which change the calculated curves considerably, are possible. The pressure side distribution for the analytical values is shifted down by 10 to 15 percent (with respect to the largest experimental value) compared to the experimental results. The reason for this displacement is probably in the choice of the initial boundary layer displacement thickness for the pressure side. The existence of a small separation bubble just after the leading edge could cause higher experimental values on the

pressure side. The lack of static pressure taps just in the region of the leading edges prevent locating such a separation bubble.

The influence of the streamtube contraction factor on the velocity distribution along the blade surface is shown in Fig. 16. An axial velocity ratio factor representing a channel height contraction factor of 1.109 was introduced into the computer program. The velocity at the leading edge increased by 10% on the suction side, whereas on the pressure side no change is registered. The channel contraction and the fact that the flow is turned by the blades explains the higher velocity at the leading edge suction side and also the general increase on the entire suction side compared to the pressure side. The influence on the profile loss is small and amounts to a four percent increase. The same change is found for the deflection angle, which decreased by 5.7 percent down to 15.5 degrees and is still one degree off the measured and averaged deflection angle of 14.5 degrees.

The variation of the total pressure loss and the deflection angle covering two blades at the center of the cascade is shown for $i = -6.0°$ in Fig. 17. This plot is qualitatively representative of all test results obtained from the wake measurements. The extraordinary development of the deflection curve is due to the velocity distribution close to the trailing edges and the relatively large dimensions of the yaw probe compared to the boundary layer or wake thickness. In fact, a total pressure gradient occurs in a direction normal to the axis

of the probe. Since the holes p_2 and p_3, being separated by a certain distance, are in regions of different total pressure, the probe must be rotated through an additional angle. An explanatory drawing is shown in Fig. 21.

The results for the mean total head losses as well as the mean deflection angles are presented in Fig. 18. The experimental data plotted show an expected behavior similar to results for a double arc compressor blade described in reference 27. The minimum loss occurs for an incidence angle approximately equal to zero. The points for double minimum loss are to be found at $i = +6.0°$ resp. $i = -7.0°$, where usually positive and negative stall can be assumed. Typical stall regions, which would induce a sharp increase in mean total head losses, are missing as previously mentioned. This is due to the presence of the endwall boundary layers which accelerate the freestream additionally within the blade passage. A comparison between calculated and measured values in Fig. 18 shows reasonable agreement at zero incidence angle. The experimental and theoretical losses differ considerably for incidence angles not equal zero. This is due to the type of velocity profiles applied in the boundary layer calculations and perhaps the method of calculating losses. Related to the deviation of the calculated losses is the difference between the two deflection angle curves. No agreement can be expected and is realized as long as the losses differ.

The effect of the freestream turbulence level on the velocity

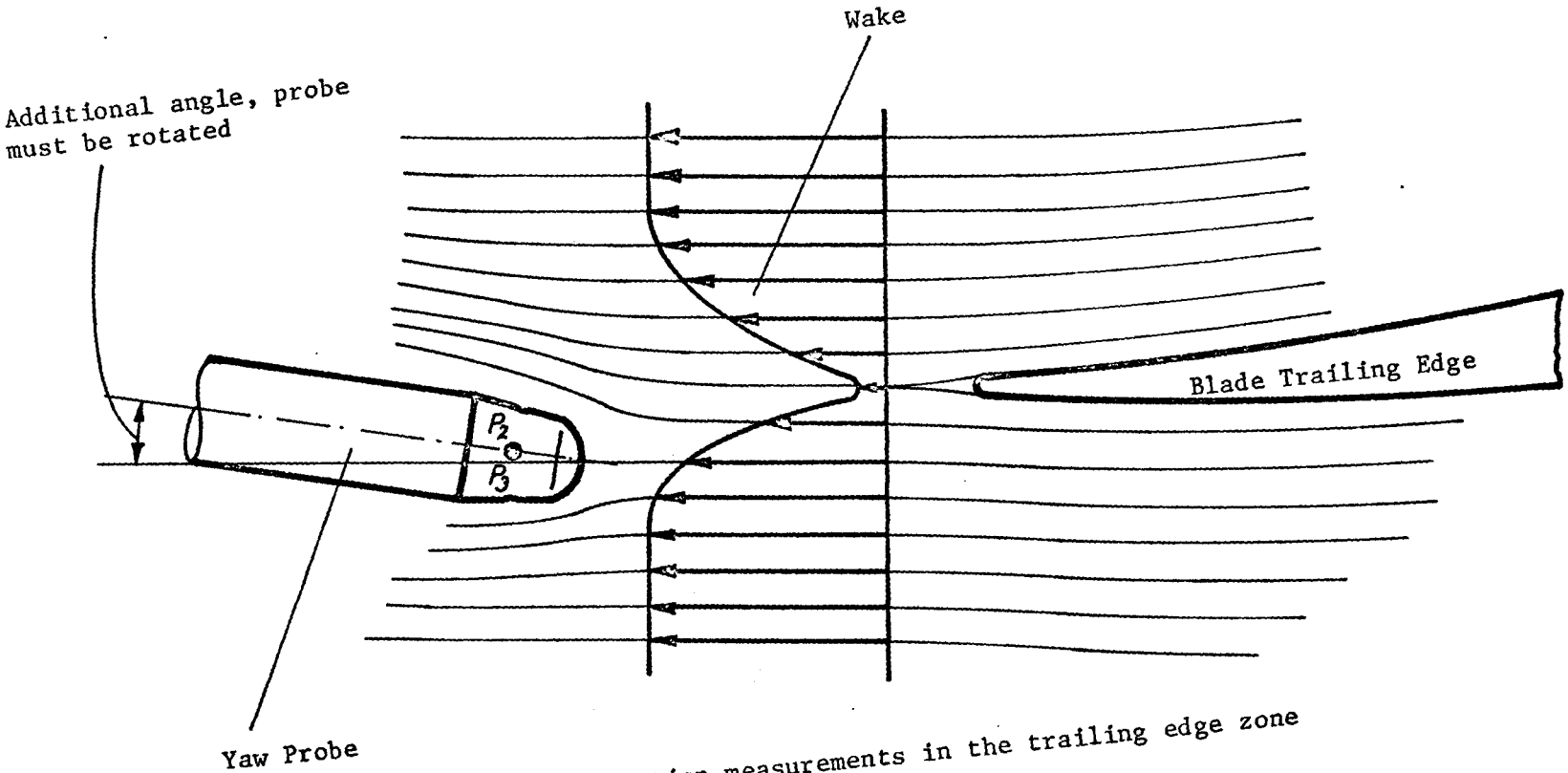

Fig. 21 Flow direction measurements in the trailing edge zone

distribution along the blade surface is clearly shown in Fig. 19. The suction side of the blade as well as the pressure side are exposed to laminar flow for the lower turbulence level (Tu = 0.61%). The characteristic step shape of the suction side velocity distribution indicates the existence of a laminar separation bubble, which starts at 40 percent of chord. The transition of the laminar boundary layer to a turbulent boundary layer is assumed to occur at the top of the bubble, shown in figure 22, which causes a reattachment of the flow before the trailing edge. No separation occurs at the pressure side. A survey of the entire range of incidence angles tested shows that the bubble length increases with decreasing incidence angle, resulting in complete separation with no reattachment at $i = -6.0°$. An incidence angle increase forces the separation bubble to disappear at $i = +6.0$ degrees without any signs of separation. This behavior of the cascade at low turbulence level explains the shape of the loss curve in Fig. 20 for Tu = 0.61 percent. A similar behavior of the mean total head loss versus incidence angle curve was found by Schlichting [26] for a NACA 65-612 profile at a Reynolds number of 1.0×10^5. Also the same behavior was reported by Andrews [27], but for a low and a high Reynolds number instead of a low and a high turbulence level. The comparison of the mean deflection angles for the two turbulence levels in Fig. 20 shows a drop in the deflection angle with increased turbulence level losses. This is clearly due to the presence of a laminar separation bubble or complete separation at the suction side of the blade.

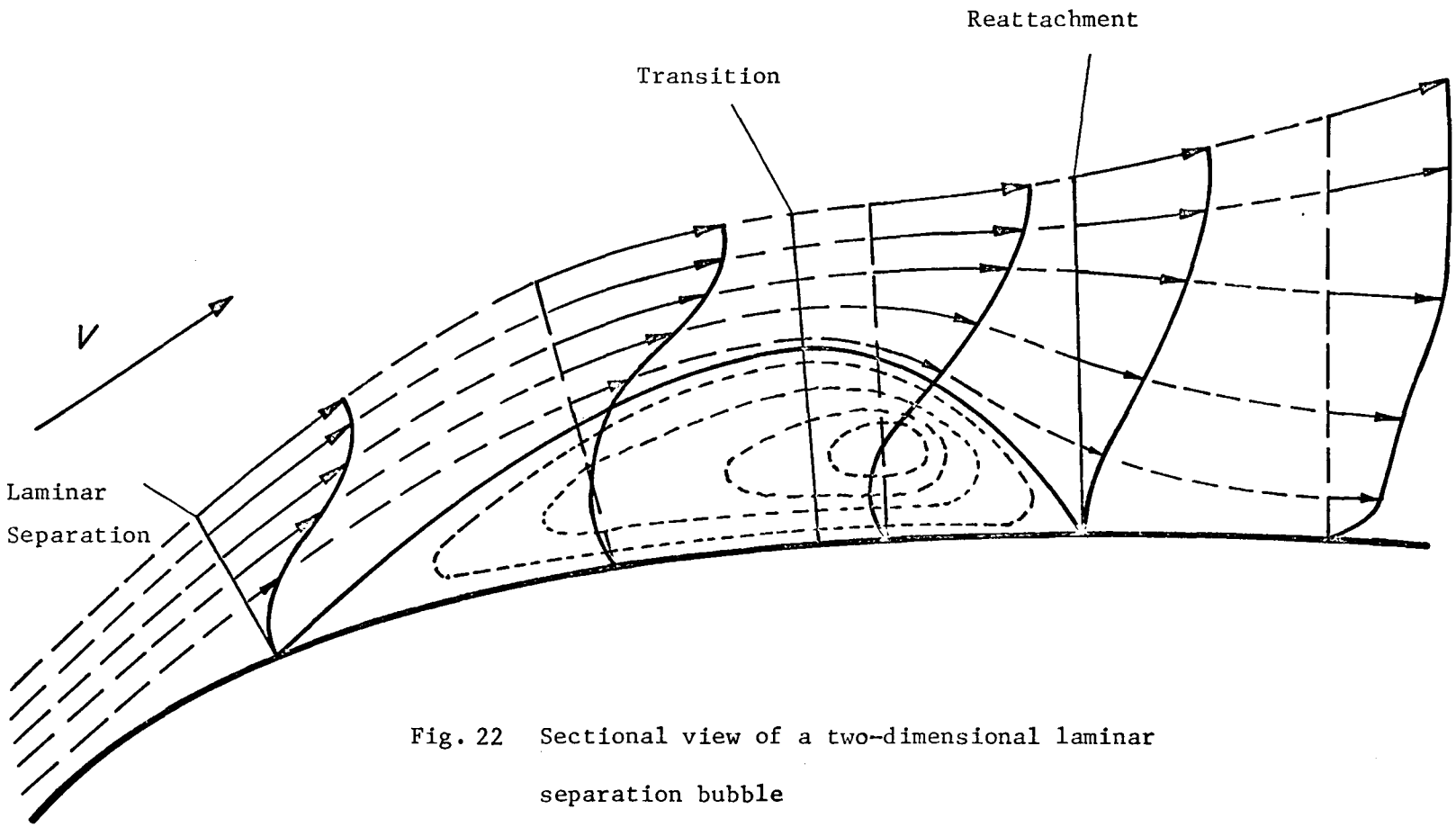

Fig. 22 Sectional view of a two-dimensional laminar separation bubble

XIII. CONCLUSIONS

A comparison between experimental and theoretical results shows that

(i) the calculated velocity distributions follow the trend established by the experimental curves,

(ii) the values for the mean total pressure losses match for zero incidence angle but diverge considerably for nonzero angles of incidence,

(iii) an agreement for the deflection angle curves cannot be expected, since the loss curves do not match and

(iv) taking into account a stream tube contraction factor to calculate the velocity distributions results in curves which are still different from the experimental values.

These results lead to the conclusion that both the experimental equipment, as well as the computer program, need improvements. This can be achieved for the cascade test section by

(i) boundary layer suction through both rotary discs one chord upstream and on one side wall, as shown in Fig. 23,

(ii) applying the so-called "tailboard technique" to adjust the flow on one side of the cascade (see Fig. 24) and

(iii) mounting static pressure taps to check the flow uniformity (see Fig. 23).

The computer program will be improved by

(i) applying a family of boundary layer velocity profiles which include backflow,

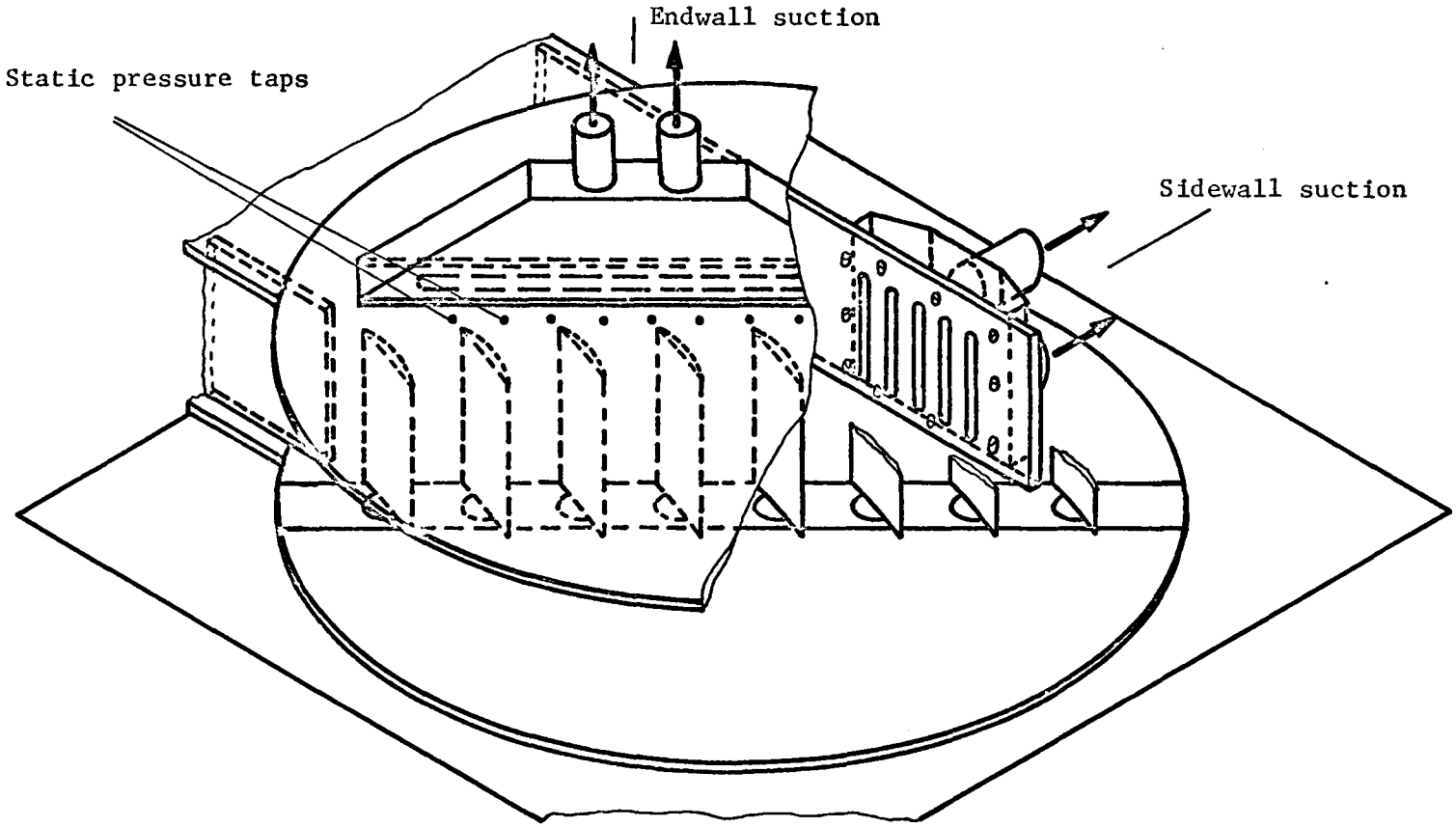

Fig. 23 Boundary layer removal apparatus and static pressure taps for uniformity check

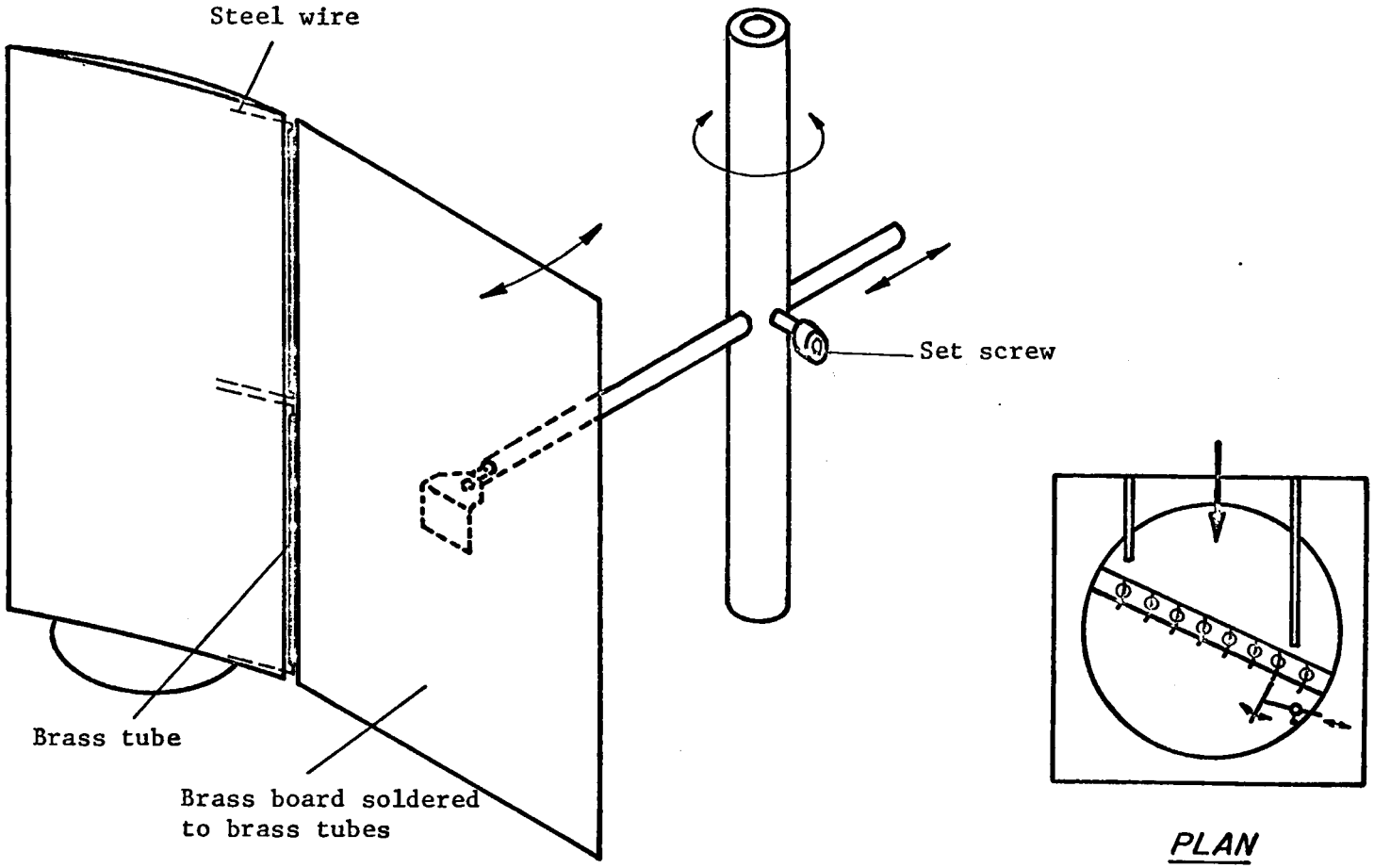

Fig. 24 Tailboard

(ii) improving the method of determining initial boundary layer values (H_{12} and δ_1) and

(iii) improving the loss calculation technique.

The experiment also indicated that, even for a low Reynolds number, turbulent flow conditions can be obtained by means of turbulence generators far upstream.

XIV. RECOMMENDATIONS

Beside the modifications listed in the foregoing chapter, further following studies should be made:

(i) A detailed investigation of the flow field and flow conditions in the improved cascade test section including flow visualization to confirm results.

(ii) Cascade tests at higher Reynolds numbers and Mach numbers to include the compressibility effect.

(iii) A comparison of the cascade tests with the computer results in the compressible region.

(iv) The inclusion of laminar boundary layer calculations in the computer program to be able to predict laminar separation bubbles as found in the present investigation for low Reynolds number and low freestream turbulence level.

XV. REFERENCES

1. Dzung, L. S. and Seippel, C., "Aerodynamic Aspects of Blading Research," published in Dzung, L. S., Flowresearch on Blading, Elsevier Publ. Comp., 1970.

2. Traupel, W., Thermische Turbomaschinen, Band I, 2nd edn., Springer, Berlin, 1966, Paragraph 8.1.

3. Keller, U. J., "Bilanzverfahren und Guetebeurteilung im Dampfkraftwerkbau," Brown Boveri Report (unpublished), 1977.

4. Cohen, J., Rogers, G.F.C., and Saravanamuttoo, H.I.H., Gas Turbine Theory, 2nd Ed., London, Longman, 1972.

5. Moses, H. L., Jones III, R. R., O'Brien Jr., W. F., and Peterson, R. S., "Simultaneous Solution of the Boundary Layer and Freestream with Separated Flow," AIAA Journal, Vol 16, No. 1, January 1978, pp. 61-66.

6. Herrig, L. J., Emery, J. C., and Erwin, J. R., "Systematic Two-Dimensional Cascade Tests of NACA 65-Series Compressor Blades at Low Speeds," NACA R. M. L51G31, 1951.

7. Howell, A. R., and Carter, A. D. S., "Fluid Flow Through Cascades of Aerofoils," Rep. R. G., British NGTE, Sept. 1946.

8. Hawthorne, W. R., Aerodynamics of Turbines and Compressors, Princeton, 1964.

9. Schlichting, H., Grenzschicht-Theorie, G. Braun, Karlsruhe, fuenfte Auflage, 1964.

10. Erwin, J. R., and Emery, J. C., "Effect of Tunnel Configuration and Testing Technique on Cascade Performance," NACA Rep. 1016, 1951.

11. Carter, A. D. S., Andrews, S. J., and Shaw, H., "Some fluid dynamic research techniques," Proc. Inst. Mech. Engrs. 163 (W.E.P. 60), 1950.

12. Lieblein, S., "Experimental Flow in Two-Dimensional Cascades," NASA SP-36, 1965, pp. 183-226.

13. Pollard, D., Gostelow, J. P., "Some Experiments at Low Speed on Compressor Cascades," Journal of Engineering for Power, July, 1967, pp. 427-436.

14. Roberts, W. B., "The Effect of Reynolds Number and Laminar Separation on Axial Cascade Performance, "ASME Paper No. 74-GT-68, Journal of Engineering for Power. ASME, Series A, Vol. 97, Part 2, April, 1975.

15. Ross, R., and Bohne, P. B., "The Character of Flow Unsteadiness and its Influence on Steady State Transonic Wind Tunnel Measurements," AGARD-CP-174.

16. Horlock, J. H., Axial Flow Compressors, Fluid Mechanics and Thermodynamics, Butterworths Scientific Publications, 1958.

17. Roudebush, W. H., "Potential Flow in Two-Dimensional Cascades," SP-36, NASA, 1965.

18. Imbach, H. E., "Die Berechnung der kompressiblen, reibungsfreien Unterschallstroemung durch raeumliche Gitter aus Schaufeln auch grosser Dicke und starker Woelbung," Mitt. Inst. Thermische Turbomaschinen ETH Zuerich, 1964.

19. Van den Braembusch, R. A., "Calculation of Compressible Subsonic Flow in Cascades with Varying Blade Heights," von Karman Institute for Fluid Dynamics, Belgium, May 1973.

20. Katsanis, T., and McNally, W. D., "Fortran Program for Calculating Velocities and Streamlines on a Blade-to-Blade Stream Surface of a Tandem Blade Turbomachine," TN D-5044, Nasa, 1969.

21. Jones III, R. R., "The Analytical Evaluation of the Performance of a Single Stage Axial Flow Compressor with Experimental Comparison," Ph.D. thesis, Virginia Polytechnic Institute and State University, to be published in December 1978.

22. Moses, H. L., "A Strip-Integral Method for Predicting the Behavior of Turbulent Boundary Layers, Computation of Turbulent Boundary Layers -- AFOSR-IFP-Stanford 1968 Conference, Stanford University, 1969, Vol. 91, No. 3, September, 1969, pp. 475-478.

23. Stephens, H. E., "Application of Supercritical Airfoil Technology to Compressor Cascades: Comparison of Theoretical and Experimental Results," AIAA Paper No. 78-1138, July, 1978.

24. Emerson & Cuming, Inc., Canton Mass. 02021, "ECCOSLIP 122S - Silicone-based grease," Technical Bulletin 20-12, Revised 2-71.

25. Emerson & Cuming, Inc., Canton Mass. 02021, "STYCAST 1266," Technical Bulletin 7-2-26C, Revised 9/77.

26. Schlichting, H., and Das, H., "Aerodynamic Losses of Axial Turbomachines," published in Dzung, L. S., Flowresearch on Blading, Elsevier Publ. Comp., 1970.

27. Andrews, S. J., "Tests Related to the Effect of Profile Shape and Chamber-Line on Compressor Cascade Performance," Reports and Memoranda No. 2743, NASA, Oct., 1949.

XVI. APPENDICES

A. General Remarks about the Determination of the Blade Cross Section and the Mold Design

In order to duplicate the real compressor blade cross section under investigation, it was necessary to determine precise geometric information about the blade contour at midspan. Since this information was not available, a real blade was cut at midspan. Afterwards, the blade contour was magnified by a factor of ten and measured with an accuracy of 0.02 millimetre. This scaling and measuring procedure was carried out by means of a comparator. A mathematical anlaysis of the resulting contour showed that the midspan cross section of the blade has very nearly a double-arc shape.

All the data were scaled such that the final chord length of the blade to be produced is two times the chord length of the real blade cross section. Generally, a larger chord length increases the accuracy of the experimental data. The final cascade blade data are shown in Fig. 3 and Fig. A1.

The material used to produce the blade mold was chosen to be aluminum. A machine that had the capacity to mill a radius of 361.06 millimetres for the pressure side part of the mold was not available. A simple and satisfactory solution was found by approximating the pressure side contour by means of a bent metal sheet. The deviations of the dimensions resulting from this solution are within ± 0.05 millimetre. No difficulties were encountered in the production of the mold part for the suction side (radius = 103.61 mm).

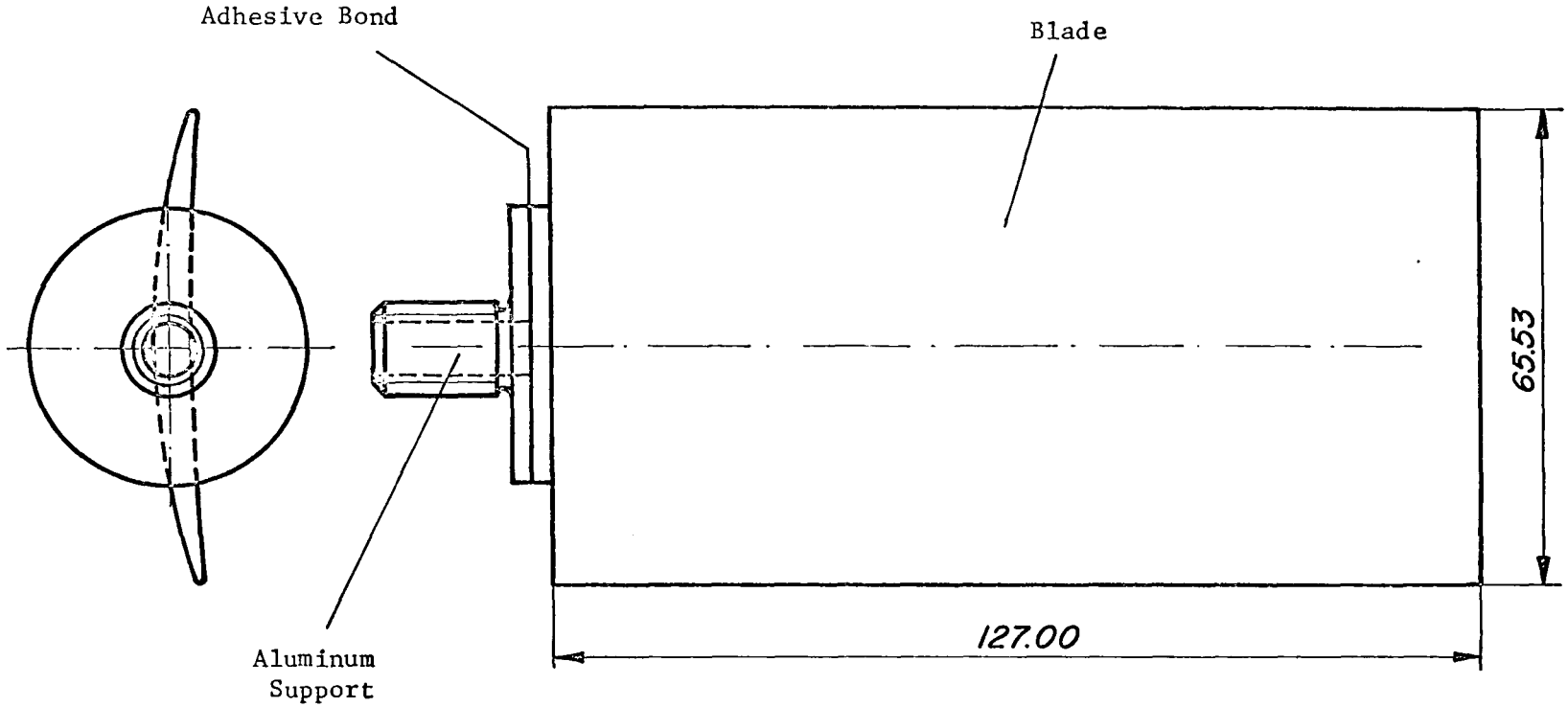

Fig. A1 Cascade blade bonded to aluminum support

B. Description of the Blade Mold

The blade mold consists of three major parts:

(i) the mold part for the suction side,

(ii) the mold part for the pressure side, and

(iii) the ground plate.

Beside these mold components, responsible for the blade shape, three dowel pins, four allen screws and two countersunk screws are used to assemble the mold. After a blade is cured in the mold, there are four hex-head screws which make the separation of the suction and pressure side part easy. A pictorial view of all mentioned components is shown in Fig. A2.

C. Description of the Blade Production

To get the mold ready for casting a blade, all the parts have to be cleaned with spirit process fluid 24-2030. All mold surfaces, invisible after the assembling, have to be wiped with mold release grease by means of a clean cloth. The grease, described in reference 24, can be obtained from Emerson & Cuming, Inc., Canton, Mass. 02021. The mold surfaces, responsible for the final blade shape, have to be polished carefully to guarantee a smooth blade surface. Before mounting the suction side part on the pressure side part, three pieces of polyester cloth are placed on the pressure side of the mold as shown in Fig. A3. Afterwards, the suction side is mounted on the pressure side part and locked against shifting by means of the longer dowel pin. It has to be ascertained that the capital letters A, stamped on

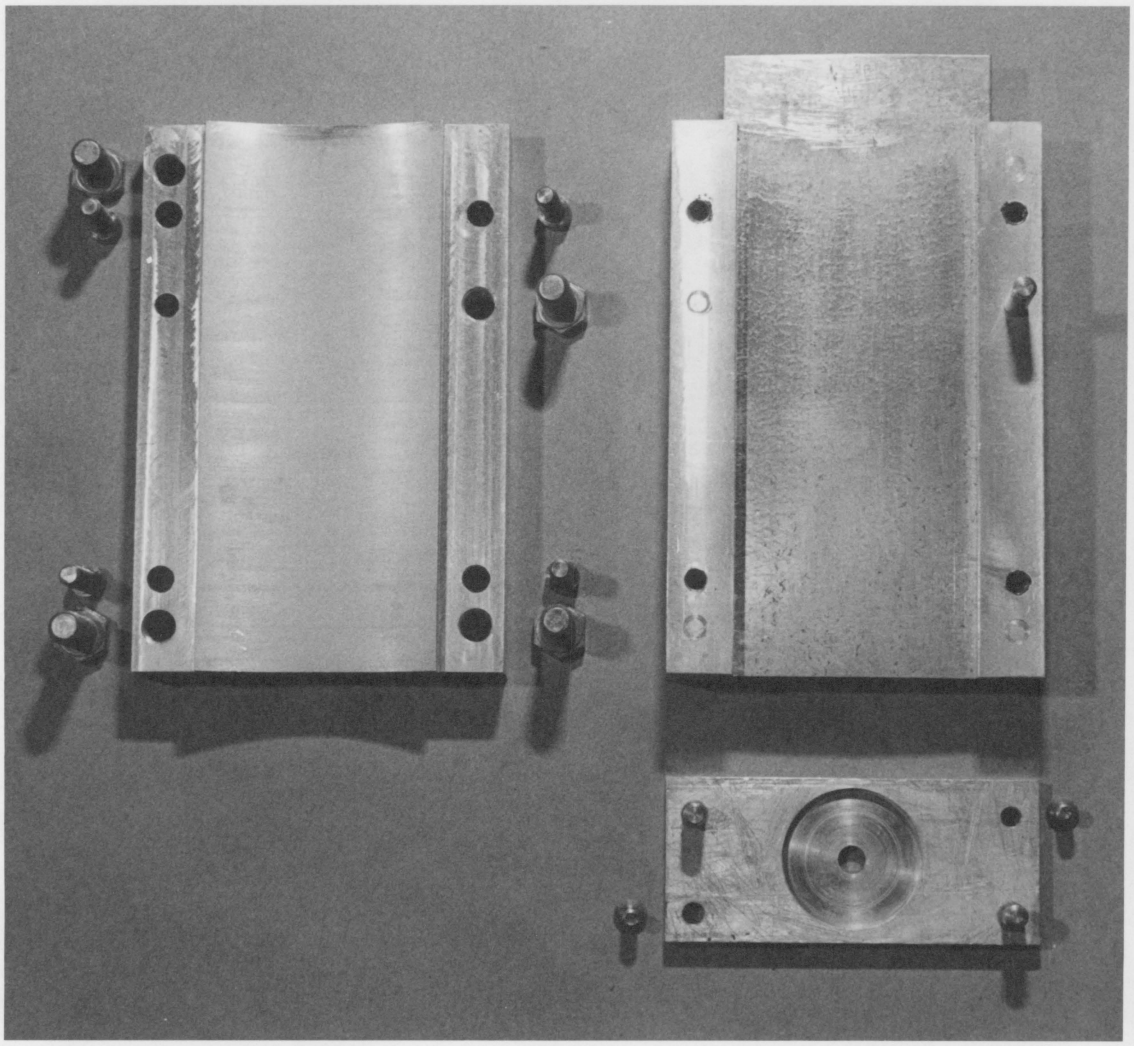

Fig. A2 Mold parts

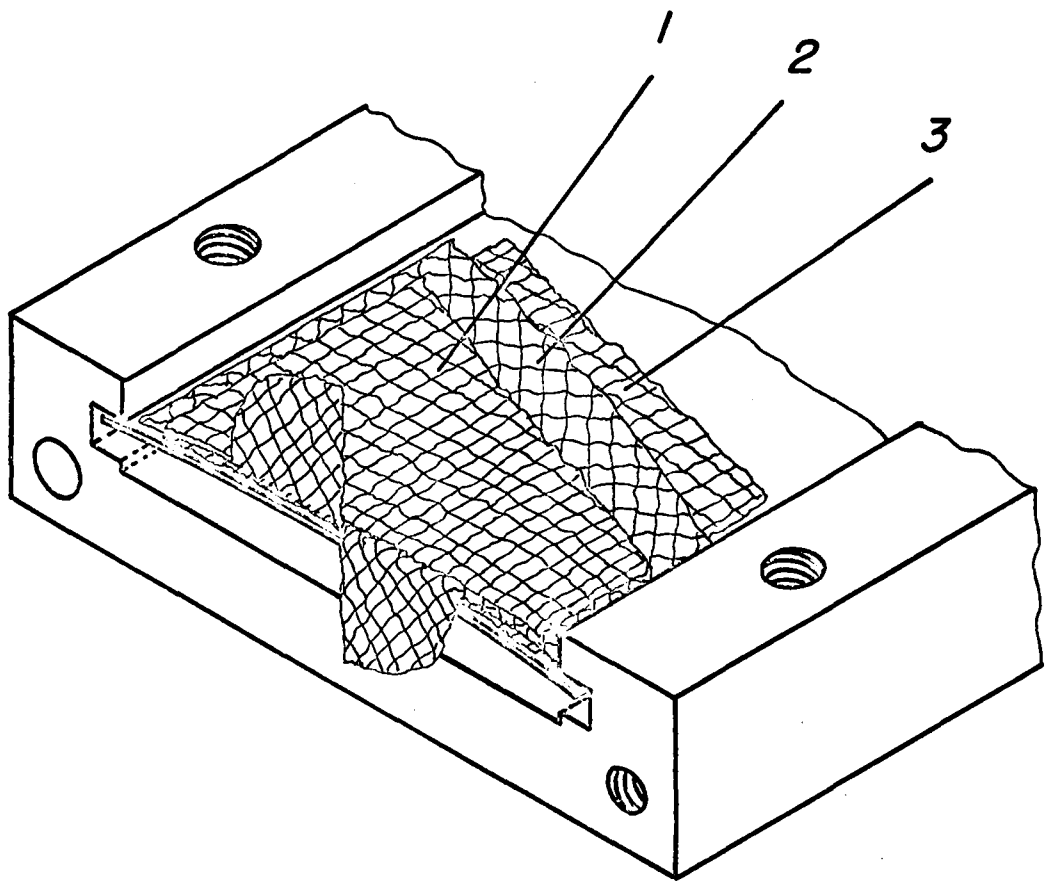

Dimensions for polyester cloth 1 and 3

Dimensions for polyester cloth 2

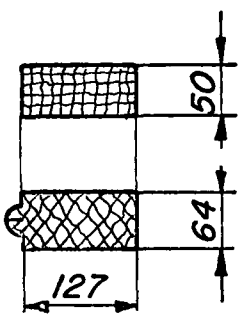

Fig. A3 Polyester cloths on pressure side part of the mold

each part, match on the same side. Four allen screws finally hold the two parts together. The center hole in the ground plate has to be sealed with putty and closed outside by means of a piece of tape. A polyester cloth of circular shape is placed in the cylindrical area in the ground plate and the plate is mounted on the assembled parts of the mold. It is of great importance that the letters B, stamped on the groundplate and on the suction side part of the mold match. Two small dowel pins keep the ground plate in the correct position while tightening the two counter sunk screws. Both pins have afterwards to be removed. The assembled mold has to be placed vertically on an even surface and the joint between the ground plate and the other two mold parts have to be sealed with putty. This step is taken to prevent the mold from leaking. A pictorial view of the mold, now ready to be filled with resin, is shown in Fig. A4. The resin, described in reference 25 consists of two parts: Part A and Part B. 28 parts of part B have to be added to 100 parts by weight of part A. This means for a blade without pressure leadings, 14 grams of part B to 50 grams of part A. In order to get a perfect blade, the mixture of the two components has to be nearly exact. After the components are thoroughly mixed, the resin can be poured very slowly into the mold by means of a special nozzle. Because of the shrinking of the material, the mold was built 25 millimetres longer than the final required blade height. However, the mold has to be filled up to the top. After eight hours, the cured blade is ready to be removed. The most difficult operation starts now. All the putty, used to seal the ground plate, has to be

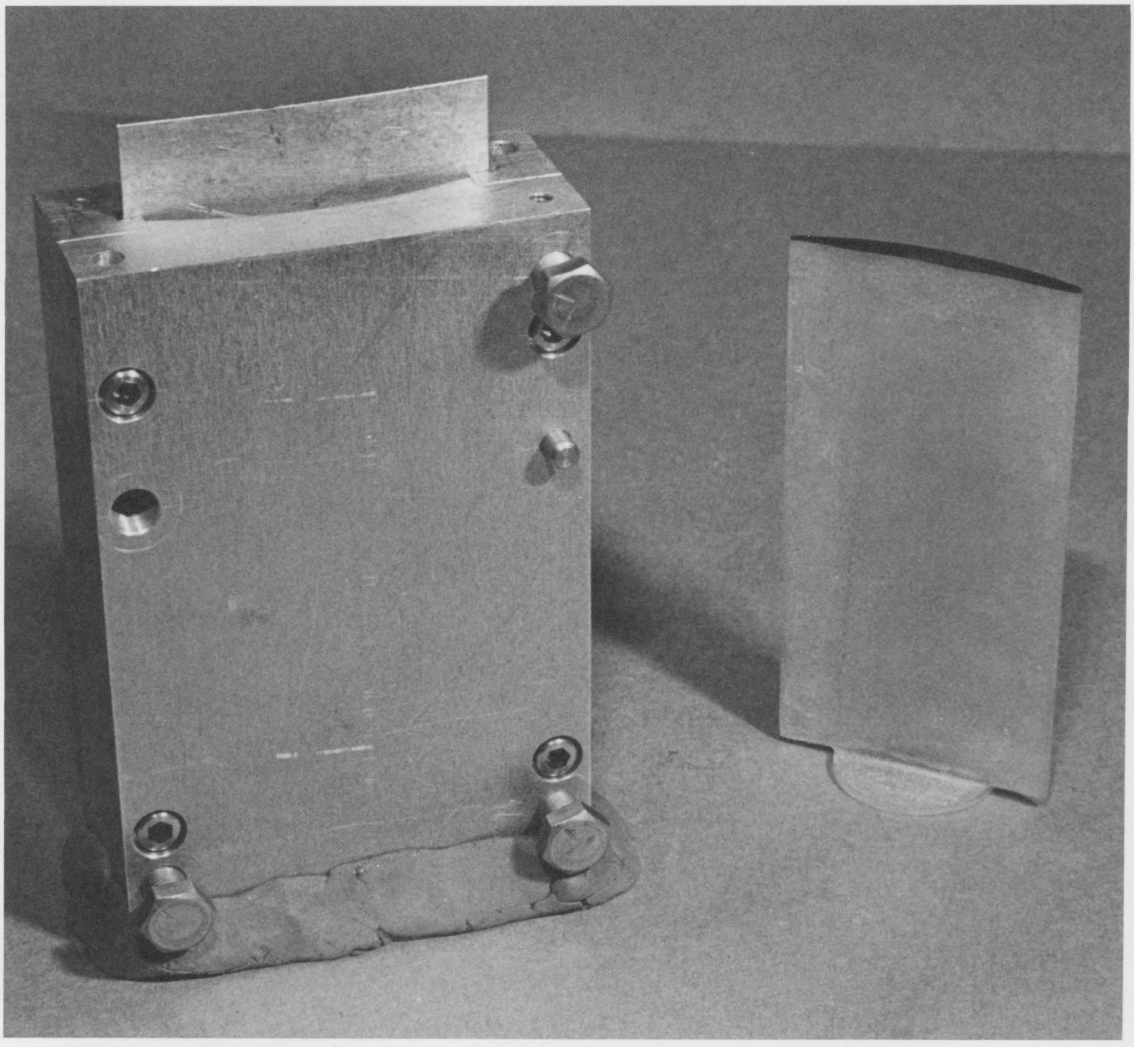

Fig. A4 Mold ready for pouring the resin, final blade

removed first. Then the outside of the mold is supposed to be cleaned. The countersunk screws holding the ground plate and the remaining two parts of the mold are removed. Applying carefully a torsional moment on the ground plate by means of a plastic hammer will make a separation of this part easy. After this step, the four hex-head screws are inserted in the corresponding threaded holes and tightened very slowly. The suction side of the mold will be separated from the cast blade which remains in the pressure side part. Starting from the bottom of the blade, the pressure side part of the mold is separated by applying pressure on the attached cylinder normal to the blade surface. This can be achieved first by means of a clamp and afterwards by inserting small balsa wood wedges between the blade pressure side and the mold. After the blade is totally removed, a reassembling of the mold with the blade inside is recommended for a final hardening process for 30 minutes under heat, supplied by a simple lamp. Then the blade is ready to be finished by repairing a few holes, originating from air bubbles, grinding the leading and trailing edges and cutting the blade at the desired height. To ascertain 100% adhesion between the blade and the aluminum support, both surfaces have to be roughened and cleaned. The application of Super Glue-X is recommended.

An almost identical procedure has to be followed for a blade with pressure leadings. After all mold parts are greased and polished, the pressure leadings, prepared on the rig shown in Fig. A5 and Fig. A6 are placed between two pieces of polyester cloth on the pressure side part of the mold. The brass tubings have an outer diameter of 1.7

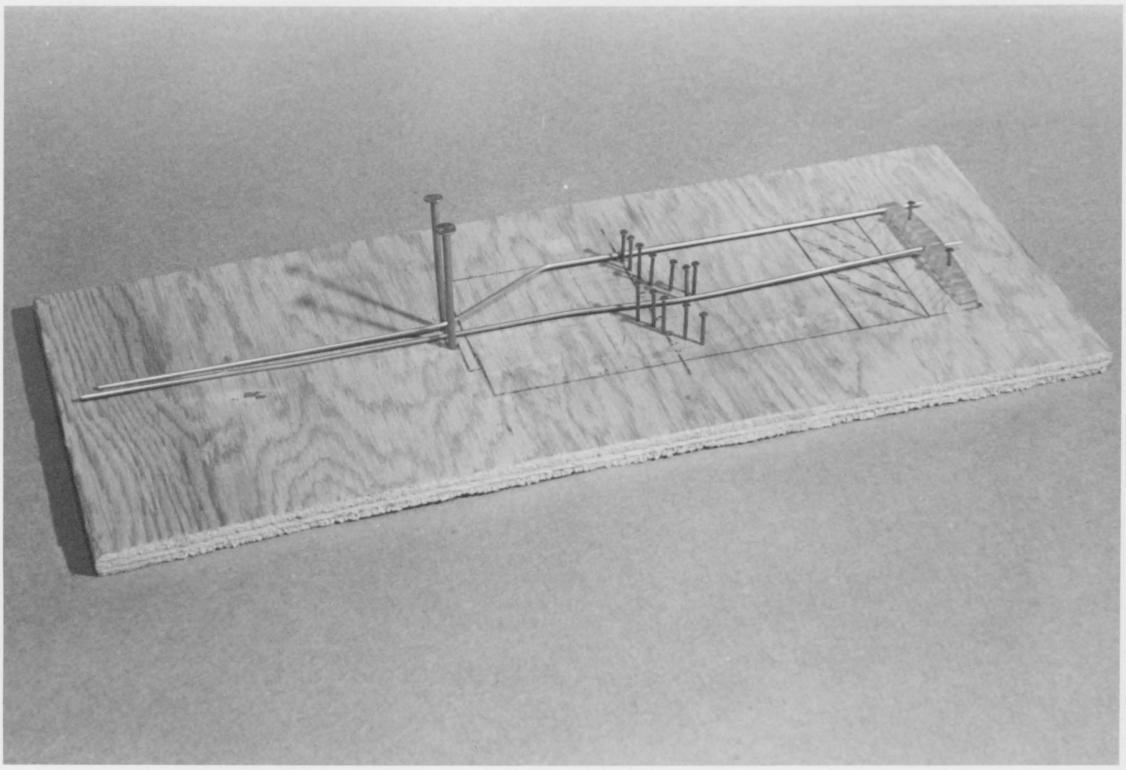

Fig. A5 Rig for pressure leadings

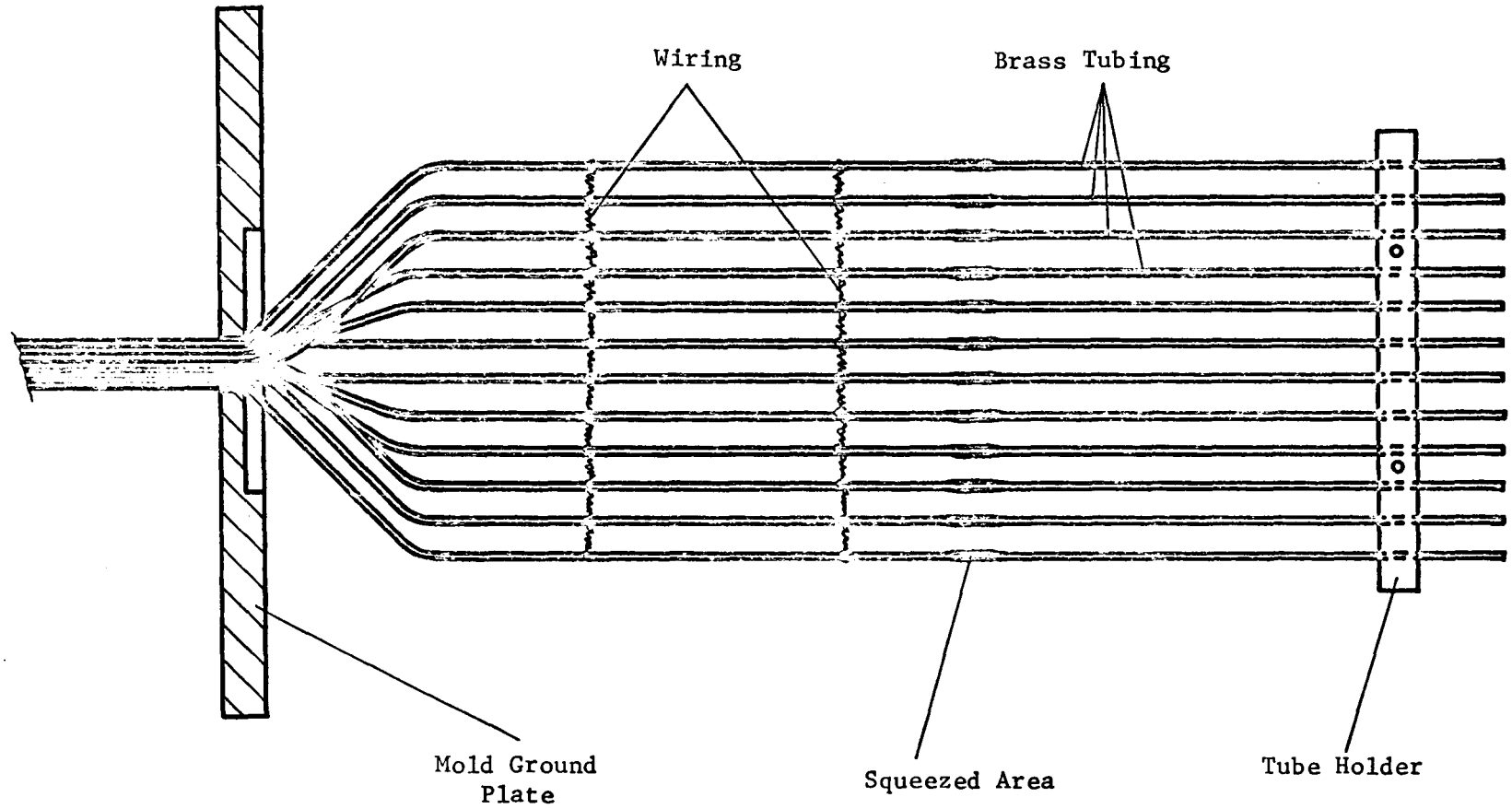

Fig. A6 Presure tubing wired and ready to be mounted on pressure side part of the blade mold

millimetres. The application of the same kind or steel tubings with a smaller outer diameter is recommended. When the mold is assembled, the tubing can be finally adjusted from the top by shifting and clambing the tubing holder on the lengthened metal sheet of the pressure side part of the mold. The hold in the ground plate, where the tubings come out, has to be sealed with putty very well. So has the joint between the ground plate and the remaining parts of the mold after the entire structure is placed vertically on a small slot, e.g. between two desks of equal height. Reassuring, that the mold is assembled correctly (capital letters A resp. B match), the blade production can be continued using a reduced amount of 12.6 grams of part B and 45 grams of part A to mix the resin. After the blade is cut at the desired height, the tubings have to be sealed from the top of the blade. First of all, putty has to be stuffed into the leadings down to the region where the tubings have been squeezed (see Fig. A6). Afterwards the openings are sealed with glue or the same resin already used for the blades. Now the pressure taps can be drilled directly from outside into the blade at the desired height. The fact that a tapered hole gives more precise pressure signals has to be remembered.

D. Calculation Procedure for the Experimental Profile Loss

Based on the experimental data as shown in Figure 17, the profile loss is calculated as follows.

The stagnation pressure losses, derived from the wake measurements, are plotted against the traversing distance as shown in Fig. A7. For both discrete stagnation pressure loss distributions, a cubic spline surve fit is made that leads to a continuous development of the loss. An integration of the resulting area averaged for the two and divided by the pitch leads to the final profile loss.

$$\frac{1}{2s}\int_{y_1}^{y_2}\frac{p_{01}-p_{02}}{\frac{1}{2}\rho V_1^2}\,dy = \frac{\overline{w}}{\frac{1}{2}\rho V_1^2} \qquad (10)$$

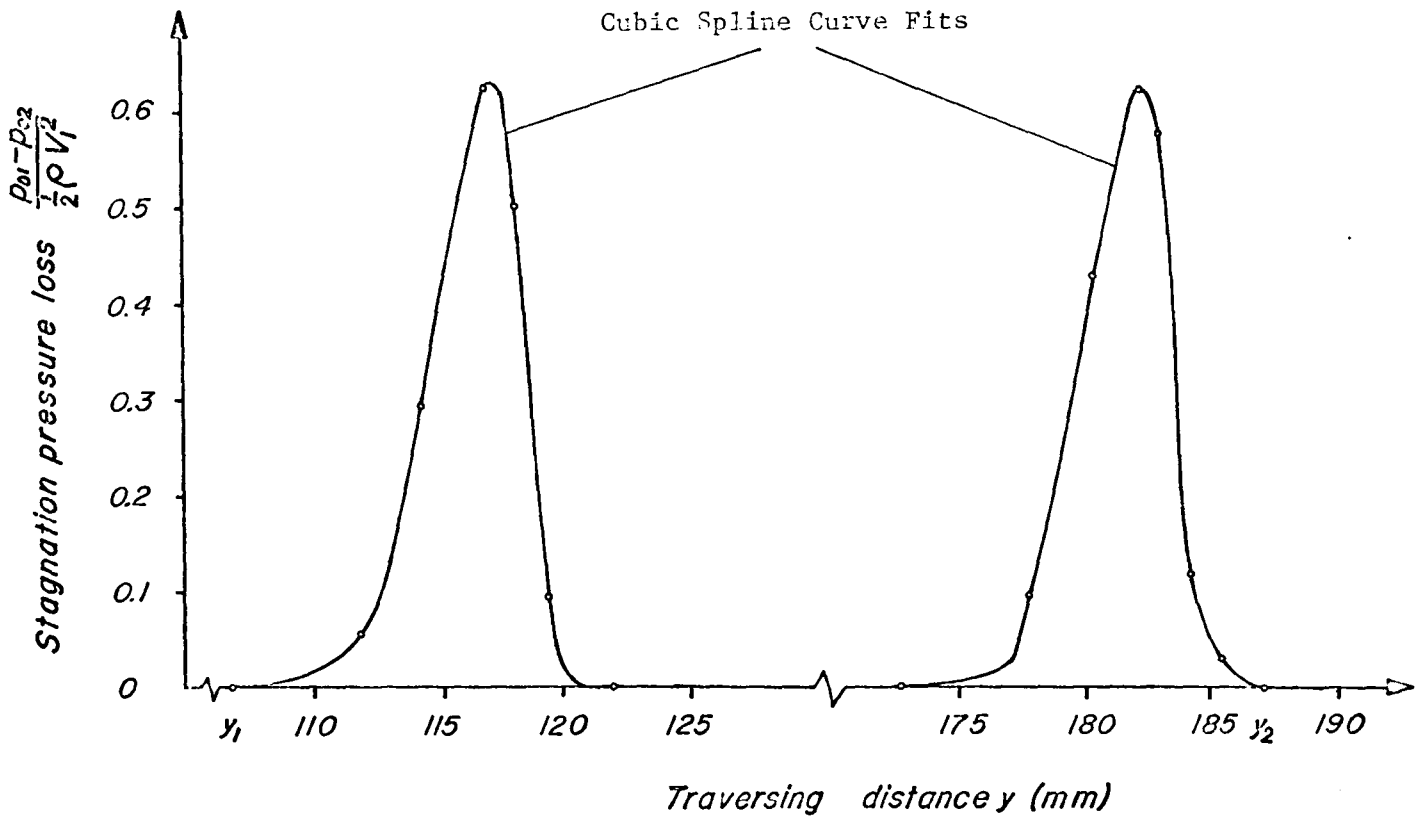

Figure A7 Stagnation pressure loss for the two center blades (example)

The vita has been removed from the scanned document

CASCADE PERFORMANCE OF A DOUBLE ARC COMPRESSOR BLADE AT LOW REYNOLDS NUMBER

by

Urs J. Keller

(ABSTRACT)

A description of a recently-developed cascade test section as well as an outline of a computer program using the simultaneous solution technique to solve the freestream and boundary layer for a quasi three-dimensional flow through a blade passage is presented. Experimental results for the velocity distributions along the blade surface, the flow deflection, and the profile loss are compared to the data obtained from the computer program for different angles of incidence.

The comparison of experimental and theoretical results is in general agreement except for the losses and deflection angles at large positive and negative incidence angles. However, the experimental equipment as well as the computer program need to be improved, since some end-wall boundary layer effects are apparent.